REPORT DOCUMENTATION PAGE

AFRL-SR-AR-TR-04-

0563

1. REPORT DATE *(DD-MM-YYYY)*	2. REPORT TYPE	3. DATES COVERED *(From - To)*
22-10-2004	**Final Performance Report**	*From August 2001-August 2004*

4. TITLE AND SUBTITLE
A Center for Organic Photonic Materials Research

5a. CONTRACT NUMBER

5b. GRANT NUMBER
F-49620-01-1-0485

5c. PROGRAM ELEMENT NUMBER

6. AUTHOR(S)
Sam Sun, Ph.D.

5d. PROJECT NUMBER

5e. TASK NUMBER

5f. WORK UNIT NUMBER

7. PERFORMING ORGANIZATION NAME(S) AND ADDRESS(ES)
Norfolk State University, 700 Park Avenue, Norfolk, VA 23504

8. PERFORMING ORGANIZATION REPORT NUMBER

9. SPONSORING / MONITORING AGENCY NAME(S) AND ADDRESS(ES)
AFOSR/NL
4015 Wilson Blvd, Room 713
Arlington, VA 22203-1954

10. SPONSOR/MONITOR'S ACRONYM(S)
AFOSR

11. SPONSOR/MONITOR'S REPORT NUMBER(S)

12. DISTRIBUTION / AVAILABILITY STATEMENT
"Approved for public release; distribution is unlimited."

13. SUPPLEMENTARY NOTES

20041109 015

14. ABSTRACT

A Center for Organic Photonic Materials Research (COPMR) was established at Norfolk State University (NSU). Novel and high efficiency optoelectronic and nano structured polymeric materials are the main research focus. Specifically, during the performance period, a series of –DBAB- type of block copolymers, where D is a conjugated electron donating block, A is a conjugated electron withdrawing acceptor block, and B is a non conjugated and flexible bridge unit, have been designed, synthesized and characterized. It was found that the photoconductivity of the synthesized –DBAB- type block copolymers was much better then the simple donor/acceptor blends under identical conditions. This was attributed mainly to the improvement in spatial domain for photo induced charge separation and transportation. Energy level domain optimizations have also been analyzed using classic electron transfer theory. These materials can be potentially developed to fabricate inexpensive, lightweight and flexible 'plastic' solar cells. Additionally, a new photo crosslinkable nonlinear optical polymer system has also been developed that may provide a photolithographic alternative for polymeric electro-optical modulator device fabrication.

15. SUBJECT TERMS

16. SECURITY CLASSIFICATION OF:			17. LIMITATION OF ABSTRACT	18. NUMBER OF PAGES	19a. NAME OF RESPONSIBLE PERSON
a. REPORT	b. ABSTRACT	c. THIS PAGE			**Sam Sun, Ph.D.**
					19b. TELEPHONE NUMBER *(include area code)* *757-823-2993*

FINAL PERFORMANCE REPORT

On

"A Center for Organic Photonic Materials Research"

AFOSR Grant #: **F-49620-01-1-0485**

PI: Sam Sun, Ph.D., Associate Professor of Chemistry and Materials Science
Center for Organic Photonic Materials Research

Norfolk State University
700 Park Avenue
Norfolk, VA 23504
Tel: 757-823-2993
Fax: 757-823-9054
Email: ssun@nsu.edu

October 31, 2004

TABLE OF CONTENTS

1. PROJECT GOALS AND OBJECTIVES

The main project goals include the establishment and strengthening of research/educational infrastructures at minority institutions that are relevant to DOD scientific/technological missions. Specific project objectives include the investigation and development of novel and improved organic and polymeric electro-active materials for efficient opto-electronic (OE) (such as photovoltaic) and electro-optical (EO) (such as nonlinear optical) applications.

2. PROJECT EXECUTIVE AND STATUS OVERVIEW

During the three-year project performance period, three tenure-track faculty, over three research faculty, and over 10 graduate/undergraduate students have been partially supported from this project. One patent relevant to the project has been filed and published, five master's degree theses relevant to this project have been defended, nearly 30 publications (including a PI edited book titled "Organic Photovoltaics: Mechanisms, Materials and Devices") have been published and is in the process of publication, and over 20 presentations (including invited lectures/seminars) have been delivered at top international level scientific communities and federal/sponsoring agencies. In addition, during the performance period, the PI and other key faculty involved in this project participated and successfully won additional major grant awards from other funding agencies such as NSF (Center for Photonic Materials Research), and NASA (Center for Research and Education in Advanced Materials). The PI won another MDA/NASA grant titled "Development of a High Efficiency and Light Weight Photovoltaic Device". Several instruments that are relevant to this project have been purchased during the performance period via other grants including Title III grants from the Department of Education. A Ph.D. program in Advanced Materials Science and Engineering is currently being drafted and is expected to be established by 2005/2006. The goals of this AFOSR project on research/educational infrastructure, and objectives on optoelectronic polymers have been accomplished significantly and leveraged by additional grants and achievements.

3. PROJECT KEY TECHNICAL ACCOMPLISHMENTS

I. NOVEL ORGANIC/POLYMERIC PHOTOVOLTAIC MATERIALS

Abstract: This study has found/concluded that the optimization of organic solar cells in both space and energy/time domains are needed in order to achieve high efficiency photoelectric energy conversion. Specifically, in the spatial domain, a 'tertiary' block copolymer supra-molecular nano structure has been designed using a –DBAB- type of block copolymer, where D is a conjugated donor block, A is a conjugated acceptor block, and B is a non-conjugated and flexible bridge unit. Several –DBAB- type block copolymers have already been designed, synthesized, characterized, and preliminarily examined for photovoltaic functions. In comparison to a simple donor/acceptor (D/A)

blend film, a corresponding -DBAB- block copolymer film exhibited much better photoluminescence (PL) quenching and photo conductivity. These are mainly attributed to the improvement in the spatial domain for charge carrier generation and transportation. With respect to the energy levels and electron transfer dynamics of these materials, this study has found the photo-induced charge separation appears to be most efficient when the donor/acceptor frontier orbital energy offset approaches the sum of the charge separation reorganization energy and the exciton binding energy. Other donor/acceptor frontier orbital energy offsets have also been identified where the charge recombination becomes most severe, and where the ratio of the charge separation rate constant over the charge recombination rate constant becomes largest. Implications and ways of achieving these optimized energy levels are briefly discussed.

1) Background of Organic Photovoltaics

Sunlight is a clean and renewable energy source conveniently available on planet earth and in outer space nearby the Sun or other shining stars. Photovoltaic materials and devices can convert light (or photon) into electricity (or mobile charges such as electrons) [1]. In addition to solar energy conversion, photovoltaic materials and devices can also be used in photo-detector applications such as in photo-electric signal transducers in optical communication or optical imaging systems. The key difference in these different applications is that, in photo-detector applications, the optical excitation energy gap (optical gap) of the photovoltaic materials must match the energy of the optical signal (*e.g.*, 1.5 micron or 0.8 eV IR light signal in optical communications). In the case of solar cells, the optical excitation gap of the material should match the solar spectrum with maximum photon flux between 1.3-2.0 eV on the surface of the earth (air mass 1.5), or 1.8-3.0 eV in outer space (air mass 0) [1-4]. Though certain inorganic semiconductor based photovoltaic materials/devices can convert about 30% of solar energy into electric power [1], in order to effectively and economically utilize Sun light for general energy needs, particularly in remote areas where large spaces are available, low cost and large area organic or polymer based solar panels or sheets are more attractive [1-14]. Though power conversion efficiencies for purely organic and "plastic" photovoltaic devices are still less then 5% [2-14], in comparison to inorganic materials, semiconducting and conducting conjugated polymers exhibit some inherent advantages such as: (1) light weight, (2) flexible shape, (3) ultra-fast (up to femtoseconds) opto-electronic response, (4) nearly continuous tunability of materials energy levels and band-gaps via molecular design and synthesis, (5) versatile materials processing and device fabrication schemes, and (6) low cost on large scale industrial manufacturing [15]. Additionally, as research in organic and polymeric photovoltaic materials are rapidly growing, key bottleneck factors, such as the 'photon losses', the 'exciton losses', and the 'carrier losses' that hinder organic/polymeric photovoltaic performance become clear [14], high efficiency organic photovoltaic systems appear to be feasible, as all these "losses" can be minimized by systematic optimization in space, energy and/or time domains. In this chapter, some fundamental mechanisms and current problems of organic photovoltaic materials and devices are briefly presented first, then spatial domain optimizations using a 'tertiary' nano structured –DBAB- type block copolymer, and energy/time domain optimizations identifying optimal donor/acceptor energy levels and offsets are described.

2) Fundamentals and Current Problems of Organic Photovoltaics

To develop high efficiency organic or polymeric photovoltaic materials and devices, a brief review and comparison of the inorganic solar cells (such as first inorganic 'Fritts Cell' [16]) versus the organic solar cells (such as first organic 'Tang Cell' [6]) is necessary. The first inorganic solar cell was described by Charles Fritts in 1885 [16]. As illustrated in Figure 1 (a), the 'Fritts' cell was composed of a semiconducting selenium thin layer sandwiched between two different metal electrodes, one very thin and semi-transparent gold layer acting as a large work function electrode (LWFE) to collect photo-generated positive charges (holes), and the other iron layer acting as a small work function electrode (SWFE) to collect photo-generated negative charges (electrons). In this cell, when an energy matched photon strikes the selenium, a loosely bound electron/hole pair was generated, the electron and hole can be separated easily by room temperature thermal energy kT (less then 0.05eV), where the free electron would be in a conduction band (CB), and the free hole is left in the valence band (VB) as shown in figure 2 (a). The free electrons and holes (also called charged 'carriers' or simply 'carriers') can then diffuse to the respective and opposite electrodes driven by a field created by the two different work function metal electrodes.

In contrast, in the first organic solar cell ('Tang Cell') as shown in figure 1 (b), when an energy-matched photon strikes an organic unit (mainly low band gaped π electron unit), it only generates a strongly bound and polarizable neutral electron-hole pair called 'exciton'. The energy required to separate the electron from the hole in an exciton, also called exciton binding energy E_B (typically in a range of 0.05-1.5 eV) is much higher than room temperature energy kT [17-19]. Such an exciton can diffuse (*e.g.*, via energy transfer) randomly within a distance defined by its lifetime of typically picoseconds to nanoseconds. The average exciton diffusion length (AEDL) for organic conjugated materials is typically 5-70 nm [17-19]. The schematic frontier orbital energy levels are shown in more detail in Figures 3 and 4. Figure 3 shows the schematic diagram of the band structure of an organic binary light harvesting system. Figure 4 shows the same system from the perspective of the Gibbs free energy. As shown in Figures 1-b, 2-b and 3, if two different organic materials with different frontier electronic orbitals are present and in direct contact to each other, one material, the "donor" has a smaller ionization potential (IP), and the other material, the "acceptor", has a larger electron affinity (EA) (Figures 2b and 3), when an exciton (in either donor or acceptor) diffuses to a donor/acceptor interface, the frontier orbital level offset between the donor and the acceptor would induce electron transfer across the interface. If the exciton is at donor side, the electron at the donor LUMO will quickly transfer into the acceptor LUMO (transfer #3 in Figures 3 and 4). If the exciton is at acceptor side, the hole at acceptor HOMO will jump quickly into the donor HOMO (corresponding to an electron back transfer #7 in Figures 3 and 4), thus an exciton now becomes a free electron (at acceptor LUMO) and a free hole (at donor HOMO) resulting in an electron-hole charge separation. Now the free electrons and holes (charged carriers) can diffuse to their respective electrodes, hopefully in two separate donor and acceptor phases, so the chance of electron-hole recombination would be minimal. Thus, a donor/acceptor binary system appears very critical for organic photovoltaic function [6].

For an organic solar cell, the overall power conversion efficiencies are determined by at least following five steps:

1) Photon absorption and exciton generation;
2) Exciton diffusion to donor/acceptor interface;
3) Exciton split or charged carrier generation at donor/acceptor interface;
4) Carrier diffusion to respective electrodes;
5) Carrier collection by the electrodes.

For all currently reported organic or polymeric photovoltaic materials and devices, none of the above mentioned five steps have been optimized. Therefore, it is not surprising that the power conversion efficiencies of all currently reported organic or polymeric solar cells are relatively low in comparison to their inorganic counterparts.

2.1) Photon absorption and exciton generation

In this first step of organic photovoltaic conversion, a basic requirement is that the materials optical excitation energy gap (optical gap) should be equal or close to the incident photon energy. In most amorphous organic materials, it is difficult to form electronic band structures due to the lack of both long-range and short-range molecular order. The energy gap defaults to the difference between the frontier orbitals, *i.e.*, the Highest Occupied Molecular Orbital (HOMO) and the Lowest Unoccupied Molecular Orbital (LUMO). In organic conjugated system, HOMO is typically an occupied π bonding orbital, and LUMO is typically an unoccupied π^* anti-bonding orbital. Since an organic LUMO/HOMO excitation basically generates a tightly bound exciton instead of a free electron and hole, the "optical energy gap" is therefore used instead of the conventional "electronic energy gap" that typically refers to the energy gap between the free holes at valence band (VB) and the free electrons at conduction band (CB) in inorganic semiconducting materials (Figure 2a). In organics, the relationship of "optical gap (E_{go})" versus "electronic gap (E_{ge})" may be expressed as $E_{ge}=E_{go}+E_B$, where E_B is called exciton binding energy that represents a minimum energy needed to separate the electron from the hole in an exciton into a radical ion pair [17]. E_{go} values are usually estimated directly from optical absorption band edge, and absolute E_{ge} values may be estimated by electrochemical redox analysis. Absolute HOMO/LUMO levels may also be estimated from a 'half' electrochemical analysis in combination with the optical absorption spectroscopy. For a widely used conjugated semiconducting polymer poly-p-phenylenevinylenes 'PPV', the exciton binding energy has been reported to be in the range of 0.05-1.1 eV [17]. If valence band VB is defined as containing 'free' holes, and CB is defined as containing 'free' electrons, then for a donor/acceptor binary organic system, the self-organized or well aligned acceptor LUMO bands may then be called CB, and self-organized donor HOMO bands may then be called VB. Unfortunately, these 'bands' have not yet been materialized so far.

For solar cell applications, solar radiation spans a wide range of wavelengths with largest photon flux between 600-1000 nm (1.3-2.0 eV, on surface of the earth or 1.5 air mass) or 400-700 nm (1.8-3.0 eV, in space or air mass 0) [1-4]. For terrestrial applications, it is desirable that the band gaps of a solar cell span a range from 1.3 to 2.0 eV. This may be achieved by incorporating a series of different band gap donor/acceptor or organic dyes that absorb light in that radiation range. However, while the solar photon loss can be minimized in this manner, due to energy transfer processes where all high energy excitons will eventually become lowest energy excitons [19], the open circuit voltage (V_{oc}) of the

cell will also be reduced accordingly, as experimental studies have revealed a close correlation between the V_{oc} and the gap between the lowest acceptor LUMO and highest donor HOMO levels [20]. In reality, several widely used conjugated semiconducting polymers used in organic solar cell studies have optical gaps higher then 2.0 eV [15]. Widely used alkyloxy derivatized poly-p-phenylenevinylenes (PPV) has a typical optical gap of about 2.3-2.6 eV, well above the maximum solar photon flux range. This is why the photon absorption (or exciton generation) for PPV based solar cells are far from being optimized at AM 1.5. This 'photon loss' problem is in fact very common in almost all currently reported organic photovoltaic materials and devices. However, one advantage of organic materials is the flexibility of its energy levels. They can be fine tuned via molecular design and synthesis. Therefore, ample opportunity exists for improvement. A number of recent studies on the developments of low band gap conjugated polymers are such examples [21-23].

2.2) Exciton Diffusion

Once an organic exciton is photo generated, it typically diffuses (*e.g.*, via intra-chain or inter-chain energy transfer or 'hopping', including Förster energy transfer for a singlet exciton) to a remote site. At the same time, the exciton can decay either radiatively or non-radiatively to its ground state with typical lifetimes between picoseconds to nanoseconds [18-19]. Alternatively, in condensed phases, some excitons may be trapped in defect or impurity sites. Both exciton decay and trapping would contribute to the "exciton loss". The average distance an organic exciton can travel within its lifetime is called average exciton diffusion length (AEDL). In non-crystalline and amorphous materials, the AEDL depends heavily on the spatial property (morphology) of the materials. For most conjugated organic materials, the AEDL is typically in the range of 5-70 nm [1-3, 18-19]. The AEDL for PPV is around 10 nm [18]. Since the desired first step of photovoltaic process is that each photo-generated exciton will be able to reach the donor/acceptor interface where charge separation can occur, one way to minimize the "exciton loss" would be to make a defect free and donor/acceptor phase separated and ordered material. One example would be a donor/acceptor phase separated tertiary nano structure such that, an exciton generated at any site of the material can reach a donor/acceptor interface in all directions within the AEDL [14]. This was called a 'bulk hetero-junction' structure [7-8]. One limitation of the first organic bilayer solar cell 'Tang Cell' was that, if the donor or acceptor layer is thicker then the AEDL, excitons may not be able reach the interfacial region to separate before decay. This 'exciton loss' is a serious problem. On the other hand, if the photovoltaic active layer is too thin or much shorter then the penetration depth of the light in the material, then "photon loss' due to poor light absorption would result. This is also why 'bulk hetero-junction' type solar cells are attractive, as they not only minimize the exciton loss by increasing the donor/acceptor interface, they can also offer enough thickness for effective photon harvesting.

2.3) Exciton Separation and Charge Carrier Generation

Once an exciton arrives at a donor/acceptor interface, the potential field at the interface due to the donor/acceptor frontier orbital energy level offsets, *i.e.*, δE as shown in Figure 3 can then separate the exciton into a free electron at acceptor LUMO and a free hole at donor HOMO, provided this field or energy offset is close to its optimal value or range as

discussed in Section 4 of this chapter. This photo-induced charge separation process is also called 'photo-doping', as it is a photo-induced (in contrast to chemical or thermal induced) redox reaction between the donor and the acceptor. For a derivatized PPV donor and fullerene acceptor binary system, it has been experimentally observed that the photo-induced charge separation process at the PPV/fullerene interface was orders of magnitude faster then either the PPV exciton decay or the charge recombination [7-8]. This means, opto-electronic quantum efficiency at this interface is near unity, and a high efficiency organic photovoltaic system is feasible.

2.4) Carrier Diffusion to the Electrodes

Once the carriers, either free electrons or holes, are generated, holes need to diffuse toward the large work function electrode (LWFE), and electrons need to diffuse toward the small work function electrode (SWFE). The driving forces for the carrier diffusion may include the field created by the work function difference between the two electrodes, and a 'chemical potential' driving force [24]. 'Chemical potential' driving force may be interpreted as a density potential driving force, *i.e.*, particles tend to diffuse from a higher density domain to a lower density domain. In an organic donor/acceptor binary photovoltaic cell, the high-density electrons at the acceptor LUMO nearby the donor/acceptor interface tend to diffuse to lower electron density region within the acceptor phase, and high-density holes at the donor HOMO nearby the donor/acceptor interface tend to diffuse to the lower holes density region within the donor phase. In the 'Tang Cell' as shown in Figure 1 (b), once an exciton was separated into a free electron at acceptor side and a free hole at donor side of the D/A interface, the electron will be 'pushed' away from the interface toward the negative electrode by both the 'chemical potential' and by the field formed from the two electrode work functions. The holes will be 'pushed' toward the positive electrode by the same forces but in the opposite direction. With this chemical potential driving force, even if the two electrodes are the same, asymmetric photovoltage could still be achieved (*i.e.,* the donor HOMO would yield the positive and acceptor LUMO would yield the negative electrodes) [24]. Mid-gap state species, either impurities/defects, or intentionally doped redox species, may also facilitate the carrier diffusion as well as conductivities by providing 'hopping' sites for the electrons or holes. However, right after electron-hole is separated at the interface, they can also recombine due to both potential drop of A-LUMO/D-HOMO and the Coulomb force between the free electron and hole. Fortunately, the charge recombination rates in most cases are much slower then the charge separation rates (charge recombination rates are typically in micro to milliseconds as compared to femto/pico seconds charge separation rate) [7-8, 36], so there is an opportunity for the carriers to reach the electrodes before they recombine. Yet, in most currently reported organic solar cells, the diffusion of electrons and holes to their respective electrodes are not really fast due to poor morphology. If donor and acceptor phases are perfectly 'bicontinuous' between the two electrodes, and that all LUMO and HOMO orbitals are nicely aligned and overlapped to each other in both donor and acceptor phases, like in a molecularly self-assembled thin films or crystals, then the carriers would be able to diffuse smoothly in 'bands' toward their respective electrodes. Currently, carrier thermal 'hopping' and 'tunneling' are believed to be the dominant diffusion and conductivity mechanism for most reported organic photovoltaic systems, therefore, the "carrier loss" is

believed to be another key factor for the low efficiency of organic photovoltaic materials and devices.

2.5) Carrier Collection at the Electrodes

It has been proposed [9] that when the acceptor LUMO level matches the Fermi level of the small work function electrode (SWFE), and the donor HOMO matches the Fermi level of the large work function electrode (LWFE), an ideal 'Ohmic' contact would be established for efficient carrier collection at the electrodes. So far, there are no organic photovoltaic cells that have achieved this desired 'Ohmic' alignment due to the availability and limitations of materials and electrodes involved. There were a number of studies, however, focusing on the open circuit voltage (V_{oc}) dependence on materials LUMO/HOMO level changes, electrode Fermi levels, and chemical potential gradients [20, 24]. The carrier collection mechanisms at electrodes are relatively less studied and are not well understood. It is believed that the carrier collection loss at the electrodes is also a critical contributing factor for the low efficiency of existing organic solar cells.

3) Optimization in the Spatial Domain via a –DBAB- type block copolymer

3.1) Block Copolymers and Self-Assembled Supra-molecular Nano Structures

Block copolymer solid melts are well known to exhibit behavior similar to conventional amphiphilic systems such as lipid-water mixtures, soap, and surfactant solutions [25-26]. The covalent bond connection between distinct or different blocks imposes severe constraints on possible equilibrium states, this results unique supra-molecular nano-domain structures such as lamellae (LAM), hexagonally (HEX) packed cylinders or columns, spheres packed on a body-centered cubic lattice (BCC), hexagonally perforated layers (HPL) and at least two bi-continuous phases: the ordered bi-continuous double diamond phase (OBDD) and the gyroid phase [25-26]. The morphology of block copolymers is affected by chemical composition, block size, temperature, processing, and other factors. For a triblock copolymer, a variety of even more complex and unique morphologies can be formed and are shown in Figure 5. Clearly, the block copolymer approach to photovoltaic function offers some intrinsic advantages over the bilayer or composite/blend systems [13-14, 27-35]. An MEH-PPV/polystyrene (with partial C_{60} derivatization on polystyrene block) donor/acceptor diblock copolymer system has been synthesized, and phase separation between the two blocks was indeed observed [13]. However, the polystyrene/C_{60} acceptor block is not a conjugated chain system, and the poor electron mobility or "carrier loss" problem in polystyrene phase still remains as an issue. On the other hand, when a conjugated donor block was linked directly to a conjugated acceptor block to form a direct p-n type conjugated diblock copolymer, while energy transfer from higher gap block to lower gap block were observed, no charge separated states (which is critical for photovoltaic functions) were detected [27].

3.2) Design and Development of a –DBAB- Type Block Copolymer for a 'Tertiary' Supra-molecular Nanostructure

To address the several loss problems of organic photovoltaic discussed above, particularly the 'exciton loss' and the 'carrier loss' problems, optimization in spatial domain of the donor and acceptor materials has been investigated. Using this rationale, a photovoltaic device based on a –DBAB- type of block copolymer and its potential 'tertiary' supra-molecular nano structure was designed (Figures 6-11) [14], where D is a π electron conjugated donor block, A is a conjugated acceptor block, B is a non-conjugated and flexible bridge unit. In this structure, the HOMO level of the bridge unit is lower then the acceptor HOMO, and the bridge's LUMO level is higher then the donor LUMO (Fig. 7). With this configuration, a wide band gap energy barrier is formed between the donor and acceptor conjugated blocks on the polymer chain (Figure 7). This potential energy barrier separates the energy levels of the donor and acceptor blocks, retarding the electron-hole recombination encountered in the case of directly linked p-n type diblock conjugated copolymer system [27]. At the same time, intra-molecular or inter-molecular electron transfer or charge separation can still proceed effectively through bridge σ bonds or through space under photo-excitation [36]. Additionally, the flexibility of the bridge unit would enable the rigid donor and acceptor conjugated blocks more easily to self-assemble, phase separate, and become less susceptible to distortion of the conjugation. Since both donor and acceptor blocks are π electron conjugated chains, if they are self-assembled in planes perpendicular to the molecular plane like a π- π stacking morphology well known in all π conjugated system [15] (Figure 8), good carrier transport in both donor and acceptor phases now become feasible.

While the –DBAB- block copolymer backbone structure may be called "primary structure" (see Figure 6), the conjugated chain π orbital closely stacked and ordered morphology may therefore be called "secondary structure" (Figure 8). This "secondary structure" style has been known to dramatically enhanced carrier mobility due to improved π orbital overlap as demonstrated in ordered discotic type liquid crystalline phases [10, 37], or in derivatized and self-assembled regio-regular polythiophenes [38], or template aligned poly-p-pheylenevinylenes [39]. Most importantly, this 'secondary structure' as shown in Figure 8 is in fact favorable for the exciton diffusion in horizontal direction and charge transport in vertical direction as has been experimentally observed [39]. Finally, through the adjustment of block size, block derivatization, and thin film processing protocols, a "tertiary structure" (Figure 9) where a "bicontinuous", such as columnar (or "HEX") type of morphology of the donor and acceptor blocks is vertically aligned on top of the substrate and sandwiched between two electrodes (Figure 10a) can be obtained. Even better, a thin donor layer may be inserted between ITO and active 'HEX' layer, and a thin acceptor layer is inserted between metal electrode and active layer (Figure 10b). A diblock copolymer where a 'honey comb' type columnar structure was formed with either top or bottom of the 'honey comb' completely covered by one block has already been observed [40]. The terminal donor and acceptor layers would enable a desired asymmetry and favorable chemical potential gradient for asymmetric (selective) carrier diffusion and collection at respective electrodes [6, 14, 24]. Since the diameter of each donor or acceptor block column can be conveniently controlled via synthesis and processing to be within the

organic average exciton diffusion length (AEDL) of 5-70 nm, so that every photo-induced exciton will be in convenient reach of a donor/acceptor interface along the direction perpendicular to the columnar. At the same time, photo-generated charge carriers can diffuse more smoothly to their respective electrodes via a truly "bicontinuous" block copolymer columnar morphology. The energy domain diagram of such a spatial tertiary structure can be represented in Figure 11. Figure 11(a) shows the open circuit situation, where each nano meter sized donor phase (or column) is in contact with an acceptor phase as depicted in Figure 9. SWFE-Femi refer to the femi level of small work function electrode, and LWFE-femi refer to the femi level of large work function electrode. Figure 11(b) shows the short circuit situation, where 'band bending' occurs within each 'HEX' column. This 'band bending' also drives the charge diffusion toward their respective electrodes.

While the increased donor and acceptor interface area and phase morphology will dramatically minimize the exciton and carrier losses, it may also increase the carrier recombination at the same interfaces. However, by proper energy level manipulation via molecular engineering, the charge recombination rate can be reduced in comparison to the charge separation as discussed in Section 4 of this chapter. In many of the reported organic photovoltaic systems, the charge recombination typically occurs on the microseconds or slower timescale, which is in contrast to the ultra-fast picosecond- or femto- seconds charge separation rate at the same interface [8, 36]. Therefore, the charge carrier recombination does not appear to be of a major concern for solar cell applications where the radiation is continuous. This block copolymer photovoltaic device may be to a certain degree mimic a dye sensitized solar cell (DSSC) yet with whole donor/acceptor interface covered by photo-sensitizing dyes, and that both donor and acceptor phases are solids and 'bicontinuous'. Additionally, with appropriate adjustment of donor and acceptor block sizes and their substituents, energy levels, or with attachment of better photon energy matched sensitizing dyes on the polymer backbone, it is expected that the photon loss, the exciton loss, and the carrier loss (including charge recombination) issues can all be addressed and optimized simultaneously in one such block copolymer photovoltaic device. In order to examine the feasibility of this block copolymer solar cell design [14], a novel –DBAB- type of block copolymer (Figure 12) has been synthesized and characterized, and some opto-electronic studies have already been in progress [28-35].

3.3) Materials and Equipment, Experimental

All starting chemicals, materials, reagents and solvents were purchased from commercial sources and used directly except noted otherwise. Proton and carbon NMR data were obtained from a Bruker Avance 300 MHz spectrometer. Elemental analyses were done at Atlantic Microlab. HR-MASS and MALDI data were obtained from Mass Spectrometry facility at Emory University. Perkin-Elmer DSC-6/TGA-6 systems were used to characterize the thermal property of the materials. GPC analysis was done using a Viscotek T60A/LR40 Triple-Detector GPC system with mobile phase of THF at ambient temperature (Universal calibration based on polystyrene standards is used). UV-VIS spectra were collected from a Varian Gary-5 spectrophotometer. Luminescence spectra were obtained from a SPEX Fluoromax-3 spectrofluorometer. Electrochemical analysis was done on a BAS Epsilon-100 unit. Film thicknesses were measured on a Dektak-6M

profilometer. Thin film metal electrodes were deposited in high vacuum using a BOC-360 metal vapor deposition system. For dynamic spectroscopic studies, an Ar ion pumped and mode locked Ti-Sapphire laser system was used to create optical pulses at 800 nm and 120 femto seconds at 76 MHz. The emission from the solutions or films were spectrally filtered with a monochromator and directed on the photocathode of a streak camera with 2 ps resolution.

Figure 12 shows the chemical structures of the RO-PPV donor block (D), the SF-PPV-I acceptor block (A), the bridge units (B), and the synthetic coupling scheme of the target –DBAB- block copolymer. Specifically, the donor block RO-PPV is an alkyloxy derivatized poly-p-phenylenevinylene, and the acceptor block SF-PPV-I is an alkyl-sulfone derivatized poly-p-phenylenevinylene. Two bridge units were investigated, first one is a long dialdehyde terminated bridge Unit 1 containing ten methylene units, and the second is a short diamine terminated bridge Unit 2 containing two methylene units. When bridge unit 1 was used, both donor and acceptor blocks were synthesized with terminal phosphate groups. When diamine terminated bridge Unit 2 was used, both donor and acceptor blocks were synthesized with terminal aldehyde groups. The alkyl derivatives (R) investigated includes branched 2-ethyl-hexyl group (C_8H_{17}), the ethyl (C_2H_5) and linear decacyl ($C_{10}H_{21}$) groups. The RO-PPV/SF-PPV based block copolymer syntheses and chemical characterizations have been or are being reported separately [Appendix of this report, also references 28-29, 31, 34]. Though GPC shows a molecular size corresponding to one DBAB unit, however, due to the fact that THF insoluble higher molecular weight fractions were filtered off during GPC measurement, therefore, -DBAB- (instead of DBAB) is used for single as well as possible multiple DBAB repeating units. In this chapter, only some critical comparisons of the –DBAB- (with a two carbon diamine bridge unit 2) with a D/A blend system is presented.

3.4) Results and Discussion on Spatial Domain Optimization

As elaborated earlier, the first critical step in organic photovoltaic is a photo-induced electron transfer from the donor to the acceptor (photo-doping) as shown in Figures 1-4, and this process can be characterized by a number of techniques, including photoluminescence (PL) quenching for radiative exciton decay, light-induced conductivity (photocurrent) measurements, light induced electron spin resonance (LIESR) spectroscopy, etc [1-7]. Figure 13 shows the solution absorption spectra of the RO-PPV donor block, the SF-PPV-I acceptor block, and the –DBAB- block copolymer. Since no obvious new bands were observed in the –DBAB- absorption spectrum in comparison to D and A, therefore, there was no evidence of ground state charge transfer or 'chemical doping' in the synthesized –DBAB-. Figure 14 shows the solution PL emission spectra of the donor block, the acceptor block, and –DBAB- block in arbitrary units (because the PL emission from –DBAB- was too weak to be seen if on a same scale with D or A). From a molecular density calibrated analysis, it was found that the PL of –DBAB- was quenched by over 80% relative to pristine donor or acceptor block in dilute solution [29]. This –DBAB- PL quenching was also confirmed by a much faster PL emission decay (687 ps) of –DBAB- versus the pristine donor or acceptor decay (1600 ps) as shown in Figure 15. Since the solutions were very dilute, the probability of inter-molecular photo induced charge

separation or defect trapping is very small as the polymer chains do not interact with each other. Therefore, this > 80% PL quenching can be attributed mainly to intra-chain charge separation through the two carbon bridge unit. This intra-chain electron transfer through a bridged energy barrier has been in fact widely observed before [36, 41-42]. These results demonstrate that, a short two carbon bridge would be sufficient to separate the electronic structures of the RO-PPV donor and the SF-PPV-I acceptor block, yet it still allow effective electron transfer. Figure 16 shows the thin film absorption spectra of the RO-PPV donor block, the SF-PPV-I acceptor block, and –DBAB-. Again, no ground state electron transfer was observed. Figure 17 shows the thin film PL emission spectra of the donor block, the acceptor block, and the final –DBAB- block copolymer in arbitrary units. The PL emission of D/A blend films was similar to –DBAB-, though the amount of emission quenching varies from sample to sample, *i.e.*, very sensitive to processing conditions. Again from a molecular density calibrated PL emission analysis [29], it was found that the PL intensity of the blend films were typically quenched in the range of 10-70% relative to pristine donor or acceptor blocks, while the PL emission of the final –DBAB- films were typically quenched at 90-99%. This strong PL quenching in –DBAB- film was also confirmed by a much faster PL emission decay of the –DBAB- films as compared to the D/A blend or pristine donor or acceptor films as shown in Figure 18. It is expected that this PL quenching enhancement of –DBAB- film was mainly due the photo-induced inter-chain electron transfer from a donor block to a nearby acceptor block via close spatial contact. Clearly, such an inter-chain electron transfer enhancement is mainly due to the increase of the inter-molecular donor/acceptor interface and the improvement of the morphology of the –DBAB- block copolymer thin film. AFM and STM studies revealed no any regular pattern in a D/A blend film, yet some interesting regular pattern can be seen in –DBAB- block copolymer films [30, 32, 34]. Though details or mechanism of such pattern and its formation are unclear and are still under investigation, however, it is known that block copolymer morphology can be affected or controlled by many factors, such as chemical composition, block size, film substrates, processing conditions, etc [25-26]. Finally, a few optoelectronic thin film devices have also been fabricated and studied from these polymers. The dark current-voltage I-V curves (Figure 19) of –DBAB- and D/A blend films were compared under identical fabrication and measurement conditions (*i.e.*, same thickness, same density, etc). Figure 19 shows that the biased current (as well as calculated carrier mobility) of –DBAB- was at least two orders of magnitude better then the simple D/A blend [35]. Figure 20 shows the photo conductivity (zero bias) comparisons of –DBAB-, D/A simple blend, the commercially available MEH-PPV/C60, and dark current, all film devices were fabricated and measured under identical conditions with same molecular densities. As Figure 20 shows, the photocurrent density of –DBAB- was almost doubled then that of the D/A simple blend at absorption peak of around 400nm. The dark current is also shown at the bottom. Both the open circuit voltage (V_{oc}) and short circuit current (I_{sc}) of these devices were very small, and it was possibly due to several causes, such as un-optimized device fabrication, *e.g.*, no charge collection or injection layers were used, and probable PPV photo oxidative degradation in the air. PPV is well known for photo oxidative degradation [9]. Additionally, much larger photocurrents were initially observed when the film was irradiated in a freshly fabricated device. The values reported in the plot are the lower steady state photocurrents. It is interesting to note that the voltage biased dark current of –DBAB- was at least two orders of magnitude better then the D/A blend [35],

while the photo-current of –DBAB- was only doubled then D/A. This may be explained as follows: in biased current, sufficient and same amount of carriers were injected from the electrodes for both –DBAB- films and D/A blend films. Therefore, the orders of magnitude current density differences can only be attributed to the main difference of the two films, *i.e.,* the much better carrier transport pathways in the –DBAB- film than in the D/A blend film. However, in photocurrent measurements, even if the –DBAB- film has a much better carrier transport pathway than the D/A blend film, the photo-generated carriers may be limited in both –DBAB- and D/A films due to either limited interface sizes, improper energy levels, etc., therefore, the photocurrent difference was not as large as in biased situation. Optimizations of materials structures, energy levels, morphological controls, device fabrication and measurements are ongoing and will be discussed in the near future.

4) Optimization in the Energy/Time Domain

4.1) Background

To address the optimal energy levels in a paired donor/acceptor organic light harvesting system, first, both the donor and acceptor optical excitation energy gaps should match the intended photon energy. In solar light harvesting applications, maximum photon flux is between 1.3-2.0 eV on surface of the earth (air mass 1.5) and 1.8-3.0 eV in outer space (air mass zero) [1-4]. For optical telecommunications and signal processing, an optical band gap of 0.8 eV (for 1.55 micron IR signal) is needed. Energy gaps in both donor and acceptor should be fine tuned via molecular engineering to match the photon energy, as both can absorb photon and incur charge separation at donor/acceptor interface as shown in Figures 3-4. A critical remaining question is the magnitude of energy offset between the donor and the acceptor that is assumed to drive the charge separation. A current widely cited view is that the frontier orbital energy offset between the donor and the acceptor should be at least over the exciton binding energy E_B (*i.e.*, the minimum energy needed to overcome the electric Coulomb forces and separate the tightly bond and neutral exciton into a separate or 'free' electron and hole) [1-4, 17]. Indeed when the LUMO energy offset is too small, charge separation appears to become less efficient [43]. However, even in many positive energy offset situations (such as in electron transfer from donor to acceptor via a higher energy level bridge unit as in many DBA systems), election transfer or charge separation still occur effectively [36, 41-42, 44-45]. On the other hand, if the energy offset is too large, Marcus 'inverted' region may slow down charge separation [41-42, 44-45], and thermal ground state charge separation without photo excitation may occur, and these are not desirable for light harvesting functions. Large energy offset also reduces open circuit voltage [20]. Therefore, an analysis of optimal donor/acceptor energy offsets is necessary in order to achieve efficient charge separation, particularly in consideration of exciton decay, charge separation and recombination processes in both donor and acceptor [46-48].

4.2) Theoretical Formulation

In an 'ideal' organic donor/acceptor binary solar cell, both donor and acceptor should harvest photon and contribute to photovoltaic functions. The processes may be simplified as following (also illustrated in Figures 3 & 4):

1) Photo-excitation at donor ($D/A+h\nu_1 \rightarrow D^*/A$, D^* designates a donor exciton, $h\nu_1$ is the absorbed photon energy and can be estimated from absorption or excitation spectra).
2) Donor exciton decay to its ground state ($D^*/A \rightarrow D/A+h\nu_2$) corresponding to a standard Gibbs free energy change of E_D, decay rate constant of k_{dD}, and a reorganization energy of λ_{dD} [41-42]. $h\nu_2$ is the emitted photon energy and can be estimated from emission spectra.
3) Charge separation or electron transfer from donor LUMO to acceptor LUMO ($D^*/A \rightarrow D^+A^-$) corresponding to a standard free energy change of ΔE, electron transfer rate constant of k_{sD}, and a reorganization energy of λ_{sD}.
4) Charge recombination or electron back transfer from acceptor LUMO to donor HOMO ($D^+A^- \rightarrow D/A$) corresponding to a standard free energy change of E_D-ΔE (See Fig. 4), transfer rate constant of k_r, and a reorganization energy change of λ_r.
5) Photo excitation at acceptor ($D/A+ h\nu_3 \rightarrow D/A^*$, A^* designates an acceptor exciton).
6) Acceptor exciton decay to its ground state ($D/A^* \rightarrow DA+h\nu_4$) corresponding to a free energy change of E_A, decay rate constant of k_{dA}, and a reorganization energy of λ_{dA}.
7) Charge separation or electron transfer from donor HOMO to acceptor HOMO ($D/A^* \rightarrow D^+A^-$) corresponding to a free energy change of $E_{sA}=E_A-E_D+\Delta E$ (see Fig. 4), transfer rate constant of k_{sA}, and a reorganization energy of λ_{sA}.
8) Charge recombination, same as in process 4).

For organic solar cell purposes, the charge separated state is the desired starting point. However, charge separation (Steps 3 & 7 in Figure 3) is also competing with exciton decay (Steps 2 & 6). The ratio of charge separation rate constant versus exciton decay rate constant can therefore be defined as Exciton Quenching Parameter (EQP, mathematically represented as Y_{eq}) as:

$$Y_{eqD}=k_{sD}/k_{dD} \quad (1)$$

$$Y_{eqA}=k_{sA}/k_{dA} \quad (2)$$

for donors and acceptors, respectively. The parameter, Y_{eq} reflects the efficiency of exciton→charge conversion. It was experimentally observed that the charge separation can be orders of magnitude faster then the exciton decay in a MEH-PPV/fullerene donor/acceptor binary pair [7]. Secondly, charge separation (steps 3 & 7) is also competing with charge recombination (steps 4 & 8). The ratio of charge separation rate constant over charge recombination rate constant may therefore be defined as Recombination Quenching Parameter (RQP, mathematically represented as Y_{rq})

$$Y_{rqD}=k_{sD}/k_r \quad (3)$$

$$Y_{rqA}= k_{sA}/k_r \quad (4)$$

for donors and acceptors, respectively. For any light harvesting applications, such as solar cell applications, it is desirable that both Y_{eq} and Y_{rq} parameters are large.

From classical Marcus electron transfer theory [41-42], the electron transfer rate constants may be simplified as

$$k_{dD}= A_{dD}\, exp[-(E_D+ \lambda_{dD})^2/4\, \lambda_{dD}\, kT] \quad (5)$$

$$k_{sD}=A_{sD}\, exp[-(\Delta E+\lambda_{sD})^2/4\, \lambda_{sD}\, kT] \quad (6)$$

$$k_r=A_r\, exp[-(E_D-\Delta E +\lambda_r)^2/4\, \lambda_r\, kT] \quad (7)$$

$$k_{dA}=A_{dA}\, exp[-(E_A+\lambda_{dA})^2/4\, \lambda_{dA}\, kT] \quad (8)$$

$$k_{sA}=A_{sA}\, exp[-(E_A-E_D+ \Delta E+\lambda_{sA})^2/4\, \lambda_{sA}\, kT] \quad (9)$$

$$A_y= (2\pi H_y^2/h)(\pi/\lambda_y\, kT)^{1/2} \quad (10)$$

Where y=*dD, sD, r, dA, sA*. H_y is an electronic coupling term between two electron transfer sites and can be estimated from molecular energy and dipole parameters using Mulliken-Hush model [41-45], λ_y is the reorganization energy containing contributions from molecular motions, vibrations, solvent effects, *etc.*, and can be estimated from molecular vibrational spectroscopy or from excitation/emission spectroscopy under certain conditions [41-45]. T is temperature and k is the Boltzman constant. The standard free energy of E_D and E_A can be estimated from spectroscopic, electrochemical, and thermodynamic analysis [41-45]. When ground and photo excited states free energy potential wells have similar shapes, the following apply [36]:

$$\lambda_{dD} = (h\nu_1-h\nu_2)/2 \quad (11)$$

$$E_D = - (h\nu_1+h\nu_2)/2 \quad (12)$$

$$\lambda_{dA} = (h\nu_3-h\nu_4)/2 \quad (13)$$

$$E_A = - (h\nu_3+h\nu_4)/2 \quad (14)$$

The charge separation free energy ΔE can be approximated using Weller's equation [44-45, 49] and may be simplified as:

$$\Delta E = \delta E + E_B \quad (15)$$

Where the driving force δE is the frontier orbital (LUMO-LUMO) energy offset between the donor and acceptor (negative values), and E_B (positive values) includes all counter-driving force terms, mainly electric Coulomb forces that need to be overcome in order to separate the exciton into a stable radical ion pair. If the device external applied electric fields are negligibly smaller then the exciton binding energy or the frontier orbital energy offset, and since the exciton binding energy is generally defined as the energy needed to separate an intra-molecular exciton (D* or A*) into an inter-molecular electron-hole radical ion pair (D^+A^-), E_B therefore can also be approximated as the exciton binding energy [17].

The donor Exciton Quenching Parameter EQP can thus be expressed as:

$$Y_{eqD} = k_{sD}/k_{dD} = (H_{sD}/H_{dD})^2(\lambda_{dD}/\lambda_{sD})^{1/2} \exp(Z_{eqD}) \quad (16)$$

$$\text{Where } Z_{eqD} = -(\delta E + E_B+\lambda_{sD})^2/4\,\lambda_{sD}\,kT+(E_D+\lambda_{dD})^2/4\,\lambda_{dD}kT \quad (17)$$

The donor Recombination Quenching Parameter RQP can be expressed as:

$$Y_{rqD} = k_{sD}/k_r = (H_{sD}/H_r)^2(\lambda_r/\lambda_{sD})^{1/2} \exp(Z_{rqD}) \quad (18)$$

$$\text{Where } Z_{rqD} = -(\delta E + E_B +\lambda_{sD})^2/4\,\lambda_{sD}\,kT + (E_D -\delta E - E_B + \lambda_r)^2/4\,\lambda_r\,kT \quad (19)$$

4.3) Results and Discussion

If the frontier orbital energy offset δE is set as variable, for demonstration convenience, using temperature T=300K, k=0.000086 eV/K, and calculated (from equation 11-14) and estimated RO-PPV and SF-PPV-I data of E_D= *-2.6 eV*, E_A= *-2.7eV*, E_B = *-0.4eV*, $\lambda_{sD}=\lambda_{sA}$= *0.2 eV*, λ_r= *0.5 eV*, λ_{dD} = *0.4eV*, λ_{dA} = *0.6 eV* [29-34, 46-48], and arbitrary values H_x=*1 (x=sD, dD, sA, dA, r)*, a plot of normalized Y_{eqD}, k_r, and Y_{rqD} versus δE are shown in Figure 21.

As Figure 21 shows, when frontier LUMO orbital offset δE varies, k_r, Y_{eqD} and Y_{rqD} all exhibit their own maximum values. Using $\partial Y_{eqD}/\partial \delta E = 0$, this gives

$$\delta E_{eqD} = -\lambda_{sD} - E_B = -0.6 \text{ eV} \quad (20)$$

which corresponds to maximum donor exciton-charge conversion.

Using $\partial Y_{rqD}/\partial\ \delta E = 0$, this gives

$$\delta E_{rqD} = [2+ E_D/\lambda_r]/(1/\lambda_r-1/\lambda_{sD}) - E_B = 0.67 \text{ eV} \quad (21)$$

which corresponds to a maximum k_{sD}/k_r value.

Using $\partial\ k_r/\partial\delta E = 0$ from equation (7), this gives

$$\delta E_r = E_D + \lambda_r - E_B = = -2.5 \text{ eV} \quad (22)$$

As can be seen in Figure 21, the fastest photo-induced charge separation occurs at -0.6 eV when the RO-PPV/SF-PPV-I LUMO offset (driving force) equals the sum of charge separation reorganization energy (0.2eV) and the exciton binding energy (0.4eV, counter forces). Also, the fastest charge recombination occurs at a LUMO offset of -2.5 eV, far away from optimum charge separation offset (-0.6 eV) as well as the actual RO-PPV/SF-PPV-I offset (-0.9 eV, [32]). Therefore, charge recombination in RO-PPV/SF-PPV-I pair does not seem to be of a major concern as long as the LUMO offset is nearby the δE_{eqD}. One interesting observation was that, during the charge separation, E_B represents counter Coulomb forces, while in charge recombination, E_B represents driving Coulomb forces. Figure 21 shows recombination quenching parameter Y_{rqD} (k_{sD}/k_r) does not reach its maximum until 0.67 eV, *i.e.,* at a positive energy offset. At this positive energy offset, the photo-induced charge separation might be too slow to be attractive for efficient photovoltaic function, therefore, the δE_{rqD} value appears not important in this particular case. It is desirable that the δE_{rqD} is coincident with or close to δE_{eqD}, and that δE_{rD} is far away from δE_{eqD}.

Similarly, for acceptor, the exciton quenching parameter (Y_{eqA}) can be expressed as:

$$Y_{eqA} = k_{sA}/k_{dA} = (H_{sA}/H_{dA})^2 (\lambda_{dA}/\lambda_{sA})^{1/2} \exp(Z_{eqA}) \quad (23)$$

$$\text{Where } Z_{eqA} = -(E_A - E_D + \delta E + E_B + \lambda_{sA})^2/4\,\lambda_{sA}\,kT + (E_A + \lambda_{dA})^2/4\,\lambda_{dA}kT \quad (24)$$

using $\partial Y_{eqA}/\partial\,\delta E = 0$, this gives

$$\delta E_{eqA} = E_D - E_A - \lambda_{sA} - E_B = -0.5 \text{ eV} \quad (25)$$

corresponding to the most effective acceptor photo-induced charge separation. As a matter of fact, since the donor/acceptor HOMO offset is $E_A - (E_D - \delta E)$ (see Figure 3), from equation (25), this means most effective photo-induced charge separation at acceptor occurs where the HOMO offset equals the sum of the exciton binding energy and the acceptor charge separation reorganization energy.

For a donor/acceptor pair where both can harvest light, the exciton quenching parameter for the pair can be expressed as

$$Y_{eq(D+A)} = Y_{eqD}\,Y_{eqA} \quad (26)$$

using $\partial Y_{eq(D+A)}/\partial\,\delta E = 0$, this gives

$$\delta E_{eq(D+A)} = [(E_D - E_A)/\lambda_{sA} - 2]/(1/\lambda_{sD} + 1/\lambda_{sA}) - E_B = -0.55\ eV \quad (27)$$

The exciton quenching parameters $Y_{eq(A)}$, $Y_{eq(D)}$ and $Y_{eq(D+A)}$ versus the LUMO offset are plotted in Figure 22. As Figure 22 shows, $Y_{eq(D+A)}$ represents an overlap area where both donor and acceptor would harvest light efficiently, and the optimum offset is around -0.55 eV. The actual RO-PPV/SF-PPV-I LUMO offset of -0.9 eV appears a little larger then this optimum. Further improvement of photo-induced charge separation can be

achieved via either reducing the LUMO level of RO-PPV, or increasing the LUMO level of SF-PPV-I via molecular engineering.

Likewise, the charge recombination quenching parameter for acceptor can be expressed as:

$$Y_{rqA} = k_{sA}/k_r = (H_{sA}/H_r)^2(\lambda_r/\lambda_{sA})^{1/2} \exp(Z_{rqA}) \quad (28)$$

$$\text{Where } Z_{rqA} = -(E_A-E_D+ \delta E+E_B+\lambda_{sA})^2/4\,\lambda_{sA}\,kT + (E_D-\delta E - E_B + \lambda_r)^2/4\,\lambda_r\,kT \quad (29)$$

Using $\partial Y_{rq(A)}/\partial\,\delta E = 0$, this gives

$$\delta E_{rq(A)} = [2+(E_A-E_D)/\lambda_{sA} + E_D/\lambda_r]/(1/\lambda_r-1/\lambda_{sA}) - E_B = 0.83 \text{ eV} \quad (30)$$

This corresponds to a largest k_s/k_r ratio for light harvesting at SF-PPV-I acceptor.

For both donor and acceptor, the recombination quenching parameter can be expressed as:

$$Y_{rq(D+A)} = k_{sA}k_{sD}/k_rk_r \quad (31)$$

Using $\partial Y_{rq(D+A)}/\partial\,\delta E = 0$, this gives

$$\delta E_{rq(D+A)} = [4+(E_A-E_D)/\lambda_{sA} + 2E_D/\lambda_r]/(2/\lambda_r-1/\lambda_{sD}-1/\lambda_{sA}) - E_B = 0.75 \text{ eV} \quad (32)$$

Again, the hybrid δE value is between the donor and acceptor δE of highest Y_{rq}, and the positive value indicates the charge separation might be very slow at this offset. The $Y_{rq(D)}$, $Y_{rq(A)}$ and $Y_{rq(D+A)}$ versus δE are plotted and are shown in Figure 23.

When energy offset δE is fixed (*e.g.*, at its optimum value of -0.55 eV), and donor RO-PPV charge separation reorganization energy (λ_{sD}) is varied, as Figure 24 shows, the exciton quenching parameter $Y_{eq(D+A)}$ also experiences a maximum value. Using $\partial Y_{eq(D+A)}/\partial\lambda_{sD} = 0$, this gives

$$\lambda_{sD} \text{ (where } Y_{eq(D+A)} = \text{maximum)} = [(\delta E+E_B)^2+k^2T^2]^{1/2} - kT = 0.13 \text{ eV} \quad (30)$$

This result implies the more closer the charge separation reorganization energy toward 0.13 eV, the larger the $Y_{eq(D+A)}$ would be.

When both energy offset and charge separation reorganization energy are fixed (with λ_{sD}=0.13 eV), and charge recombination reorganization energy (λ_r) is varied, as it shows from Figure 25, the cell recombination quenching parameter $Y_{rq(D+A)}$ would experience a minimum value. Using $\partial Y_{rq\,(D+A)}/\partial\lambda_r = 0$, this gives

$$\lambda_r \text{ (where } Y_{cs\,(D+A)} = \text{minimum)} = [(E_D-\delta E- E_B)^2+k^2T^2]^{1/2} - kT = 2.42 \text{ eV} \quad (31)$$

This result implies that the more far away charge recombination reorganization energy from 2.42 eV, the larger the $Y_{rq(D+A)}$ would be.

Like in any modeling or simulation studies, the numbers used here may not be accurate or important, rather, it is the trend that is the most important and meaningful. In order to further examine this model and its predictions, a series and systematic experiments need to designed and performed. For Y_{eq} trend tests, when a donor (or acceptor) is fixed, as δE only changes k_s and not k_d, it can be regarded as a special case of 'Marcus inversion' case, and the trend has already been verified by experiments [41-42, 50]. For Y_{rq} trend tests, since δE will change both k_s and k_r, therefore, a series donor/acceptor pairs where a donor (or an acceptor) is fixed first, and then a series acceptors (or a series of donors) with different δE in relation to the fixed donor (or acceptor) need to be experimentally evaluated for their charge separation and recombination rate constants. The type of experiments described in Ref. [50] is a good example, though no charge recombination rates and related reorganization energies were given. In these experiments, it is also important that the molecular structures of the changing acceptors (or donors) are similar, so that the Coulomb force terms (or exciton binding energy) and reorganization energies are similar, and that the electronic withdrawing (or donating) strength (or δE) would be the only or major variable. In this way, δE versus the Y_{eq}, the Y_{rq} and the k_r can all be evaluated at the same time. The overall power conversion efficiency of the solar cell is expected to follow Y_{eq} more closely when both Y_{rq} and k_r are far away from Y_{eq}, and the cell efficiency can be evaluated at the same time, provided the charge transport and collection at electrodes are also similar. Unfortunately, these type of experiments have not yet been systematically performed (or are not able to be performed) at the moment due to lack of suitable materials. Finally, additional parameters and competing processes (such as other electron and energy transfer processes) may also need to be taken into account in order to have a more accurate simulation. Systematic and expanded studies, including effects from excitation energy gap changes, experimental case studies, *etc.*, are underway and will be reported in the near future.

5) Conclusions and Future Perspectives

The current low photoelectric power conversion efficiencies of organic photovoltaic materials and devices can be attributed mainly to the 'photon loss', the 'exciton loss', and the 'carrier loss' due to improper donor/acceptor energy levels/offsets and poor morphologies (spatial geometries) for the charge carrier generation, transportation, and collection at electrodes. However, high efficiency organic photovoltaic materials and devices can be achieved via optimization in both space and energy/time domains.

For optimization in the spatial domain, the key is a donor/acceptor phase separated and 'bicontinuous' morphology, where the dimension of each phase should be within the average exciton diffusion length (*e.g.*, 5-70 nm). For this reason, a –DBAB- type of block copolymer system and its potential self-assembled 'tertiary' supra-molecular nano structure has been designed and preliminarily examined. In this system, along the carrier transport direction, it is 'bicontinuous' between the two electrodes. Yet, in the plane perpendicular to the carrier transport direction, it is donor/acceptor phase separated morphology on the nanoscale, and each phase diameter is within the exciton drift distance. The much-improved PL quenching (from less then 70% to 99%), biased conductivity (two orders of improvement), and photo conductivity (two fold increase) of the synthesized –DBAB- over the simple D/A blend system is attributed mainly to morphology (spatial) improvement.

The target 'tertiary' nano structured photovoltaic device is expected to improve the photovoltaic power conversion efficiency significantly in comparison to existing organic photovoltaic devices due to the reduction of the "exciton loss" and the "carrier loss" via three-dimensional spatial optimizations (via block copolymer supra-molecular structural and morphological control).

On energy/time domain optimizations, first of all, the optical excitation energy gaps in both donor and acceptor should match the intended photon energy, and that optimal donor/acceptor energy offsets which correspond to most efficient photo-induced charge separation should be identified and materialized. Specifically, in electron transfer dynamic regime and based on Marcus theory, this study has found that, there exists an optimal donor/acceptor energy offset where exciton-charge conversion is most efficient (or exciton quenching parameter EQP reaches its maximum), and a second optimal energy offset where charge recombination is relatively slow compared to charge separation (or recombination quenching parameter RQP become largest). If the maximum RQP is too far away from maximum EQP, then this optimum RQP is insignificant as the charge separation at this maximum RQP might be too slow. The molecules should be designed and developed such that the maximum RQP is close to or coincides with maximum EQP. There also exists a third energy offset where charge recombination becomes fastest. The molecules should be designed and developed such that this maximum charge recombination is far away from maximum EQP. For a donor/acceptor binary photovoltaic system, there exists a fourth optimal donor/acceptor energy offset, where the EQP product of both donor and acceptor become largest, so that both donor and acceptor can effectively contribute to photo-induced charge separation. This final optimal donor/acceptor energy offset is related to the exciton binding energy, the optical excitation energy gaps, and the reorganization energies of the charge separation of both donors and acceptors. While there exist a desired donor (or acceptor) charge separation reorganization energy where Y_{eq} has maximum value, there also exists an undesired charge recombination reorganization energy value where Y_{rq} becomes minimum. Both the desired energy offset, the desired charge separation reorganization energy, and the undesired charge recombination reorganization energy values are critically important for molecular structure and energy level fine tuning in developing high efficiency organic light harvesting systems, including organic photovoltaic cells, photo detectors, or any artificial photo-charge synthesizers/converters.

II. A NEW CROSSLINKABLE NONLINEAR OPTICAL POLYMERS

In the EO (NLO) polymer project, research highlights include a first visible light initiated photolithographic fabrication of an NLO polymer thin film pattern (Figures 26 & 27). The significance to the field is: Photo crosslinked polymer system is an ideal system for efficient and inexpensive photolithographic fabrication of waveguide or other micro or nano structures and devices. The current commercial photolithography microstructure fabrication protocol typically employs short wavelength radiations such as UV light. Unfortunately, many organic NLO chromophores have been found chemically sensitive to UV radiation. Longer wavelength radiations, such as visible or infrared light are generally friendly to most organic NLO chromophores. Therefore, development of photolithographic fabrication protocols employing longer wavelength (including two photon micro-structure fabrication) become an important research area. In our fumarate/DR-19 derivatized NLO

polymer system (See project generated Publication #10 and Thesis #3 for details), for instance, crosslinking is initiated with visible light from a regular Halogen Lamp and NLO chromophore damage was not observed. In a typical thermally crosslinked thin film, the SHG signals of uncrosslinked PDRFC (or PDRMA) typically start to drop below 50°C, yet for the crosslinked ones, the SHG signal remains stable up to about 150°C due to chromophore dipole lock-in as reported earlier. Another significance of this system is that, unlike many previously reported crosslinked NLO polymers that typically contains NH/OH units with vibrational overtone absorptions at around 1550 nm, our NLO crosslinking polymers do not contain NH/OH units which make it very attractive in 1550 nm applications. We are also evaluating the possibility of a two-photon initiated crosslinking NLO polymer system (will be in collaboration with Professor Dalton and Professor Marder's groups), since the two-photon crosslinked system can further shift the radiation wavelength to the longer infrared region, and that the two photon crosslinking protocol can directly fabricate the desired waveguide pattern without the need of multi-step photolithographic fabrication steps.

4. FIGURES AND CAPTIONS

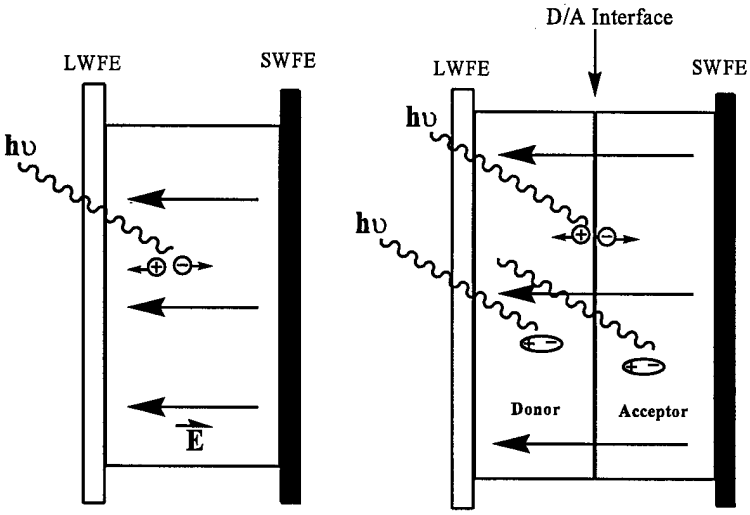

Figure 1. A schematic comparison of a classic (a) inorganic and (b) organic photovoltaic cell.

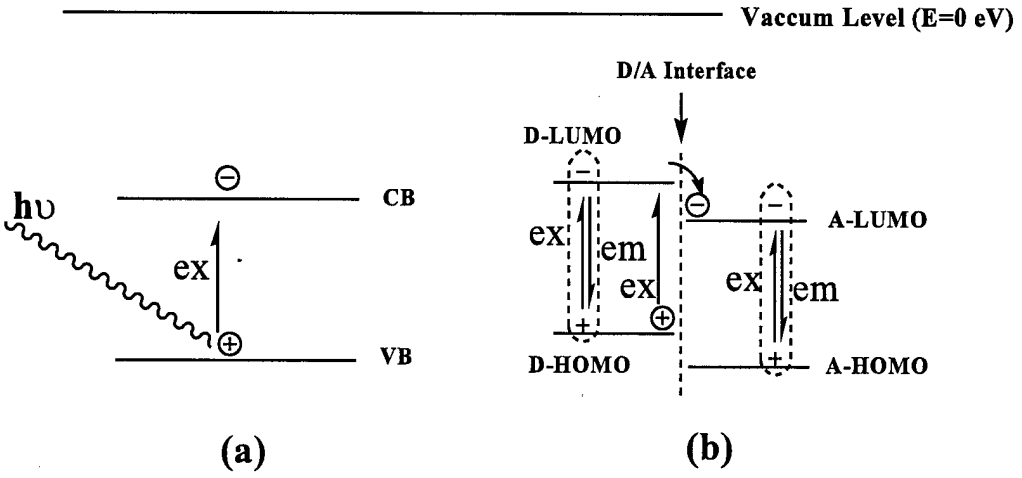

Figure 2. Schematic opto-electronic transfer processes in (a) inorganic and (b) organic photovoltaic cell. D-HOMO refers to the donor highest occupied molecular orbital, and D-LUMO refers to the donor lowest unoccupied molecular orbital, A-HOMO refers to the acceptor highest occupied molecular orbital, and A-LUMO refers to the acceptor lowest unoccupied molecular orbital. Ex means photo excitation, and Em means photo emission.

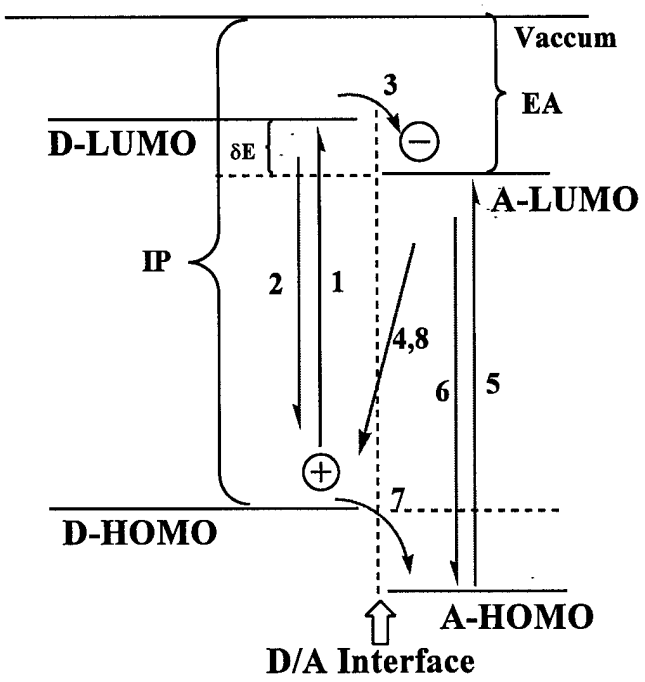

Figure 3. Scheme of molecular frontier orbitals and photo-induced charge separation and recombination processes in an organic donor/acceptor binary light harvesting system.

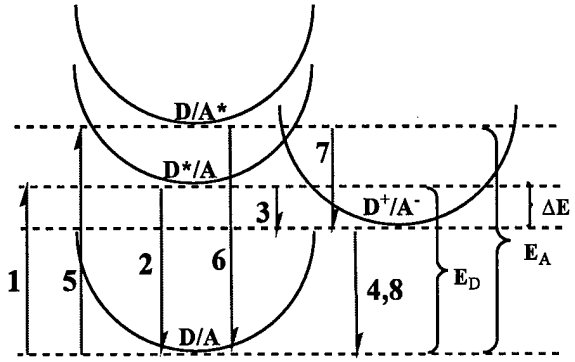

Figure 4. Scheme of standard Gibbs free-energy potential wells of photo-induced charge separation and recombination processes in an organic donor/acceptor light harvesting system.

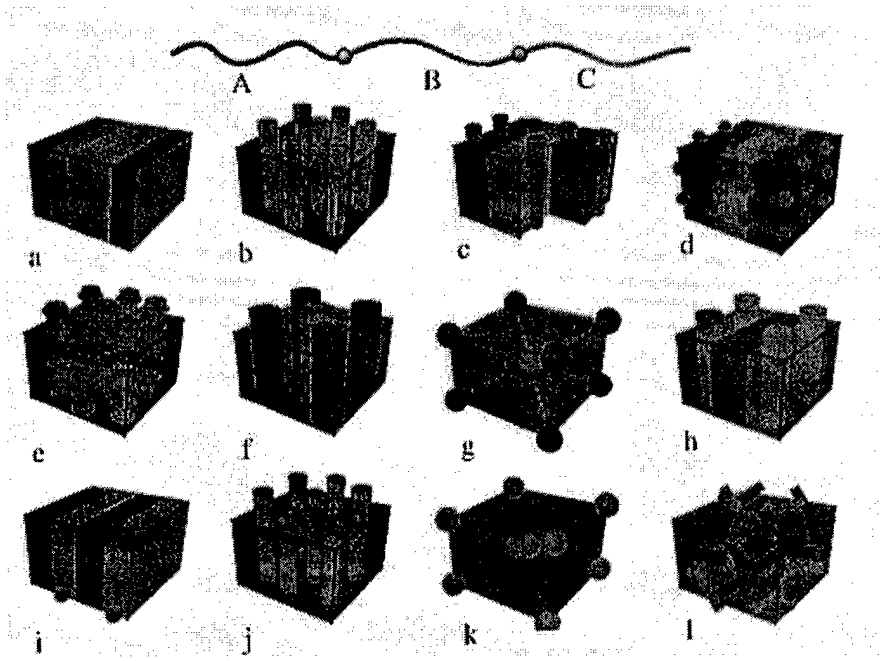

Figure 5. Representative self-assembled supra-molecular nano structures from a triblock copolymer (From Ref. 25).

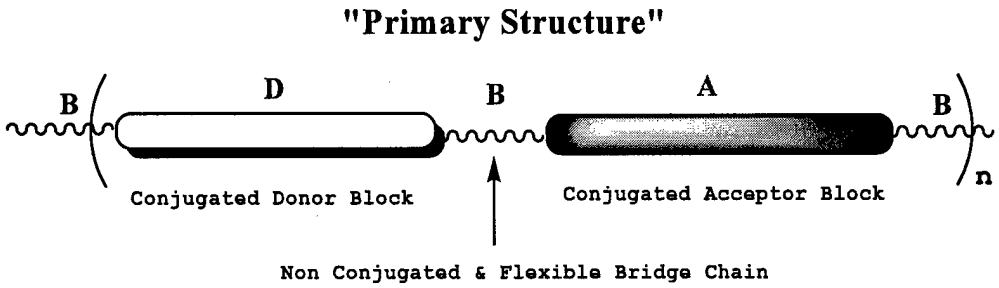

Figure 6. Scheme of a –DBAB- type of block copolymer "primary structure".

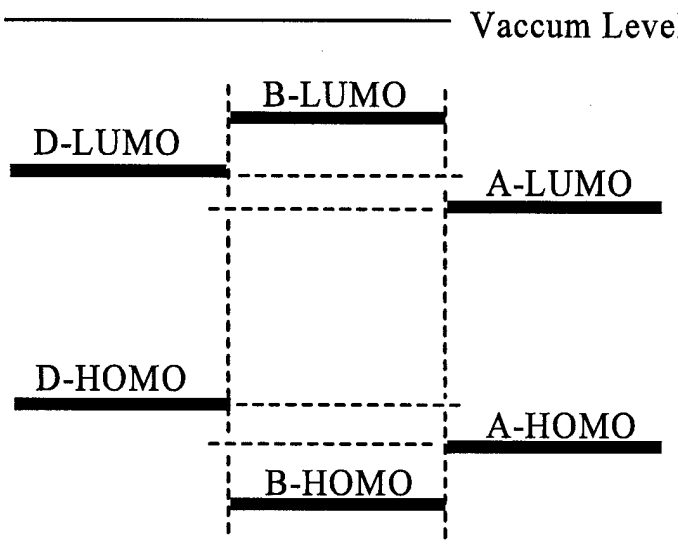

Figure 7. Scheme of a –DBAB- type of block copolymer relative energy levels.

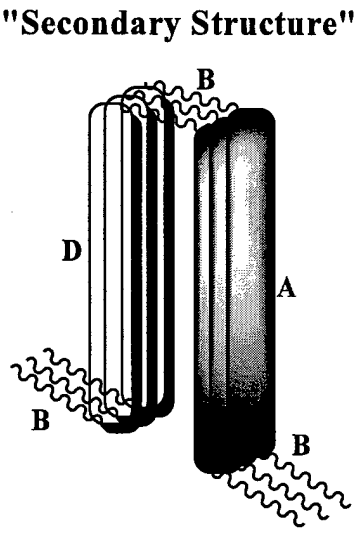

Figure 8. Scheme of a –DBAB- type of block copolymer "secondary structure".

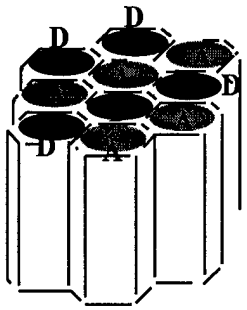

Figure 9. Scheme of a –DBAB- type of block copolymer "tertiary structure".

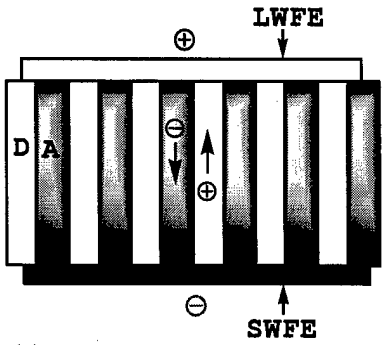

(a)

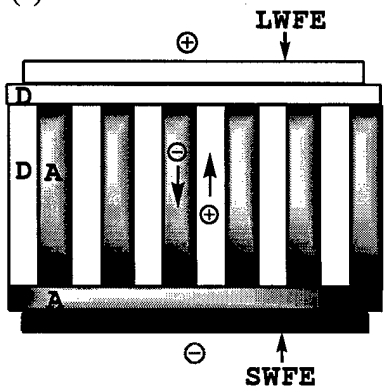

(b)

Figure 10. Scheme of a –DBAB- type of block copolymer solar cell in the form of (a) columnar structure directly sandwiched between two electrode layers and
(b) with terminal asymmetric active materials layers.

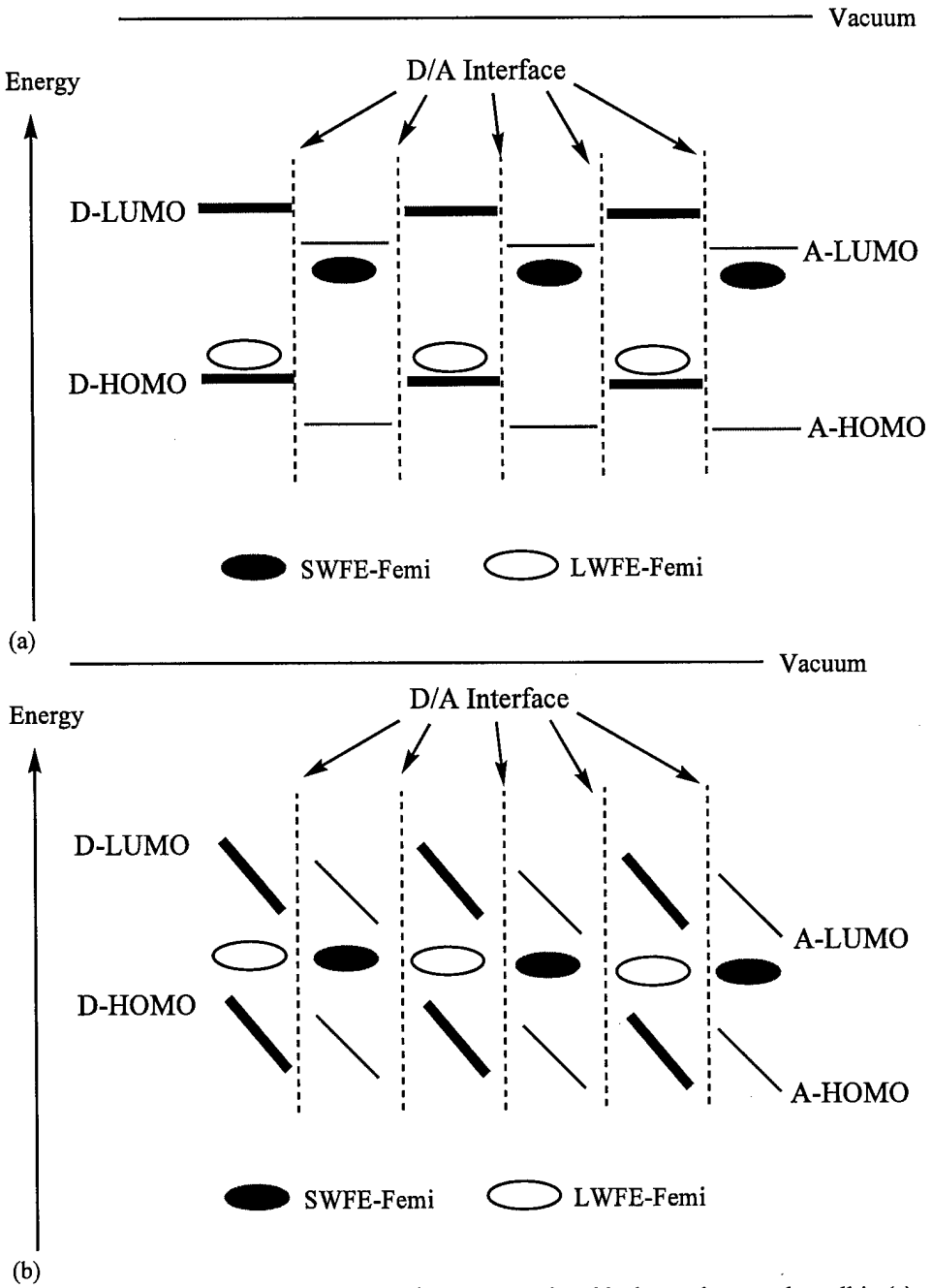

Figure 11. Schematic energy diagram of a 'HEX' tertiary block copolymer solar cell in (a) open circuit situation and (b) short circuit situation.

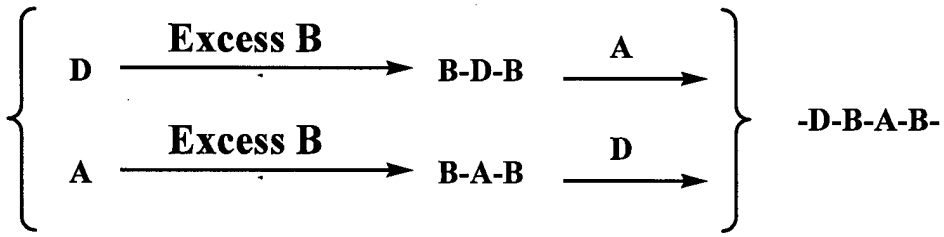

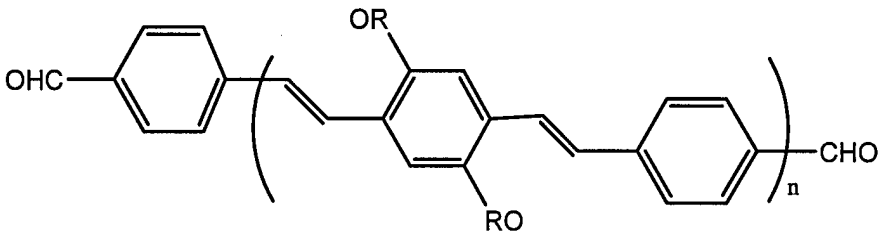

D = Donor Block

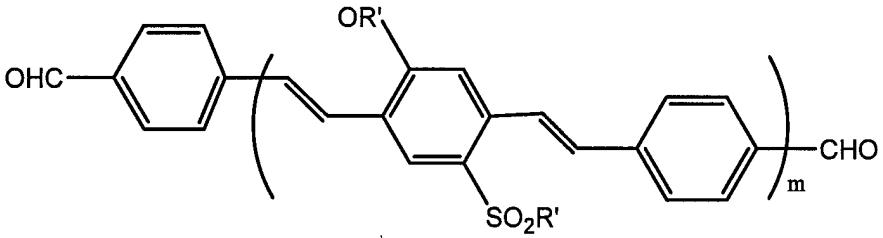

A = Acceptor Block

$R = C_{10}H_{21}$, $R' = C_2H_5$

$H_2N\text{-}(CH_2)_p\text{-}NH_2$

Bridge Unit

(a)

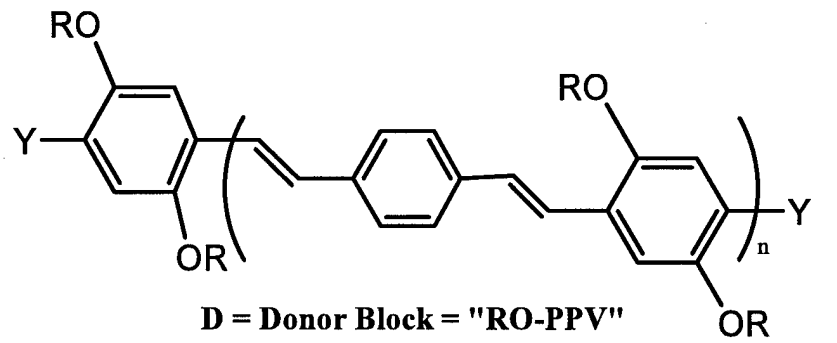

D = Donor Block = "RO-PPV"

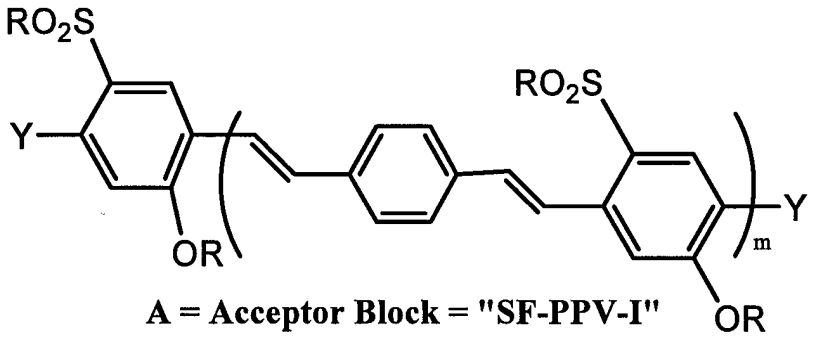

A = Acceptor Block = "SF-PPV-I"

R = $C_{10}H_{21}$, C_8H_{17}, C_2H_5, Y = $CH_2PO(OC_2H_5)_2$

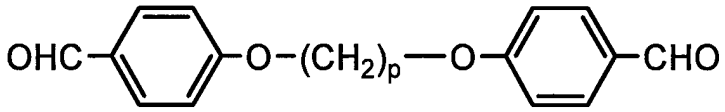

B=Bridge Unit

(b)

Figure 12. –DBAB- type conjugated block copolymer system already studied with (a) a diamine bridge unit and (b) a dialdehyde bridge unit.

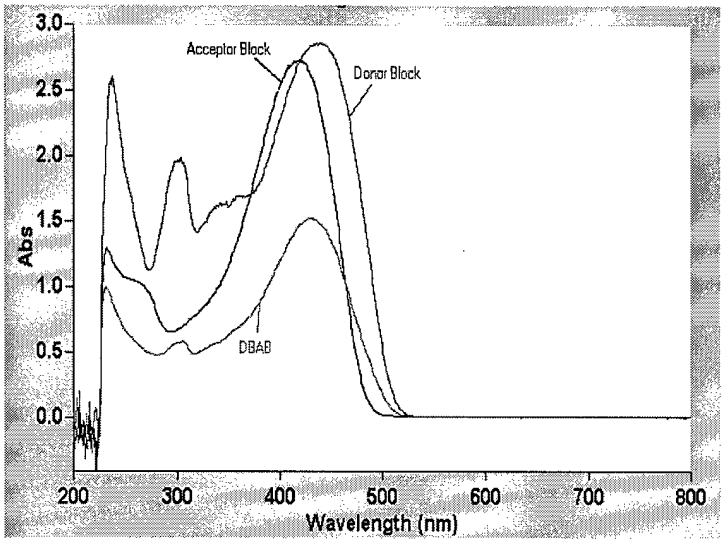

Figure 13. UV-VIS absorptions of RO-PPV (Donor), SF-PPV-I (Acceptor) and –DBAB- in dichloromethane dilute solution.

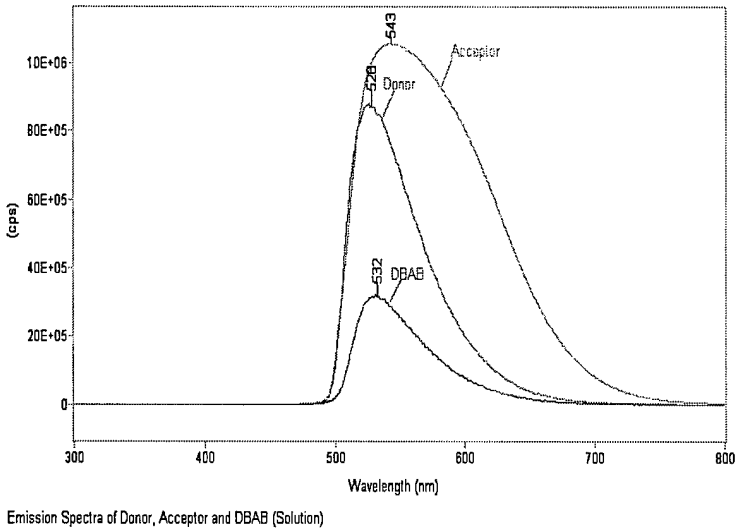

Figure 14. PL emissions of RO-PPV (D), SF-PPV-I (A), and –DBAB- in dichloromethane dilute solution. The PL intensity (y-axis) is arbitrary.

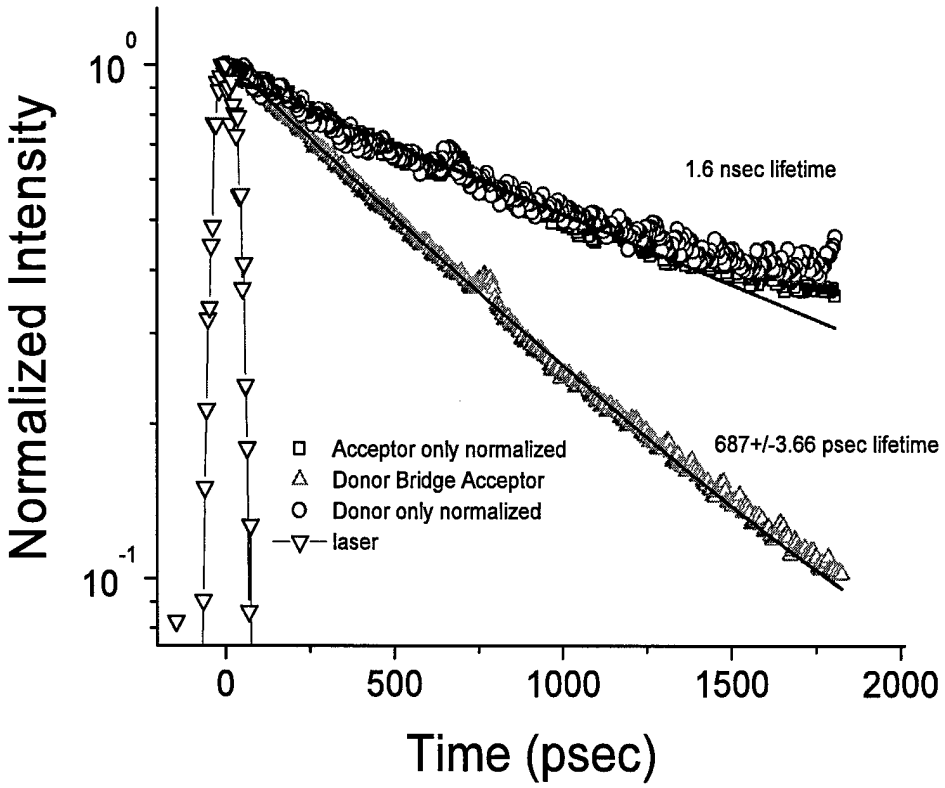

Figure 15. PL Emission Dynamics of RO-PPV (Donor), SF-PPV-I (Acceptor), and –DBAB- in dichloromethane dilute solution.

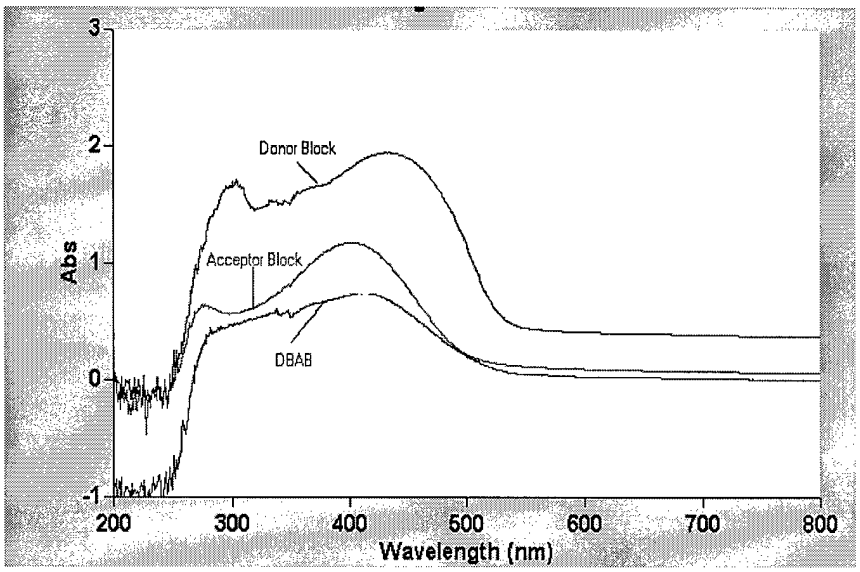

Figure 16. UV-VIS of RO-PPV (Donor), SF-PPV-I (Acceptor) and –DBAB- films on glass substrates.

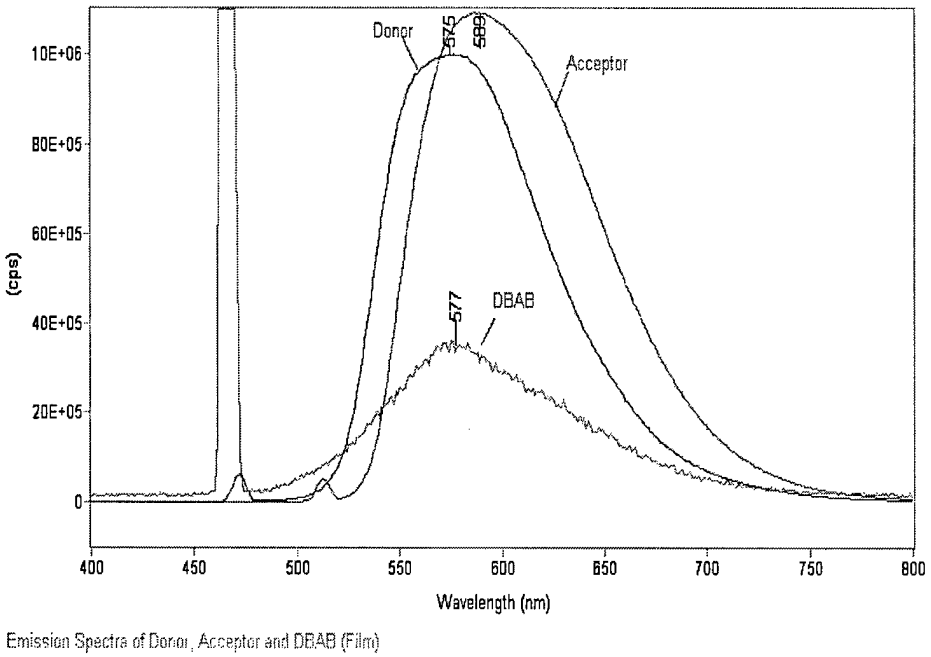

Figure 17. PL emissions of RO-PPV (D), SF-PPV (A), and –DBAB- in thin films on glass substrates. The PL intensity (y-axis) is arbitrary for better view. (Note: the spikes at 470 nm and 510 nm are due to reflected excitation beam).

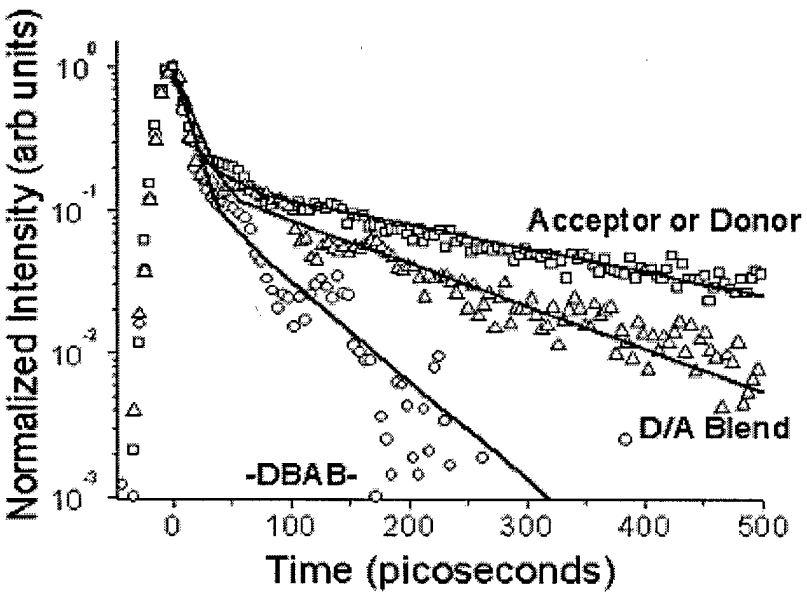

Figure 18. PL Emission Dynamics of RO-PPV (Donor), SF-PPV-I (Acceptor), and –DBAB- in films on glass substrates.

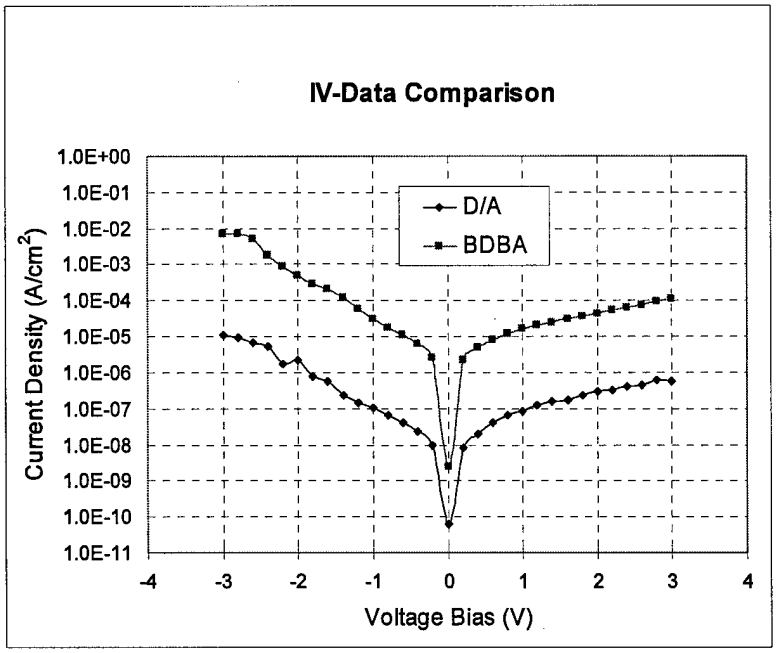

Figure 19. Voltage biased electric current density from thin films of –DBAB- block copolymer and D/A blend. Both films have the same materials density, same thickness and same electrode area.

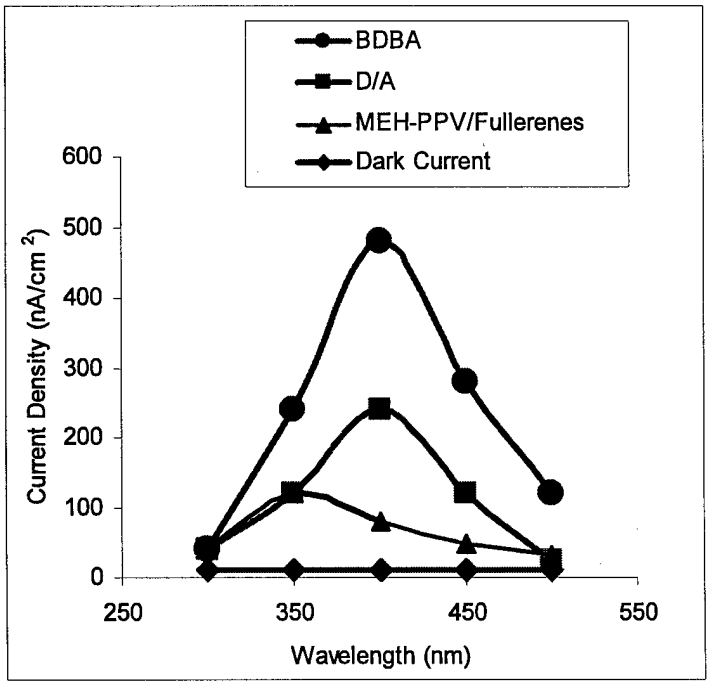

Figure 20. Photo current comparisons of several organic thin film photovoltaic cells.

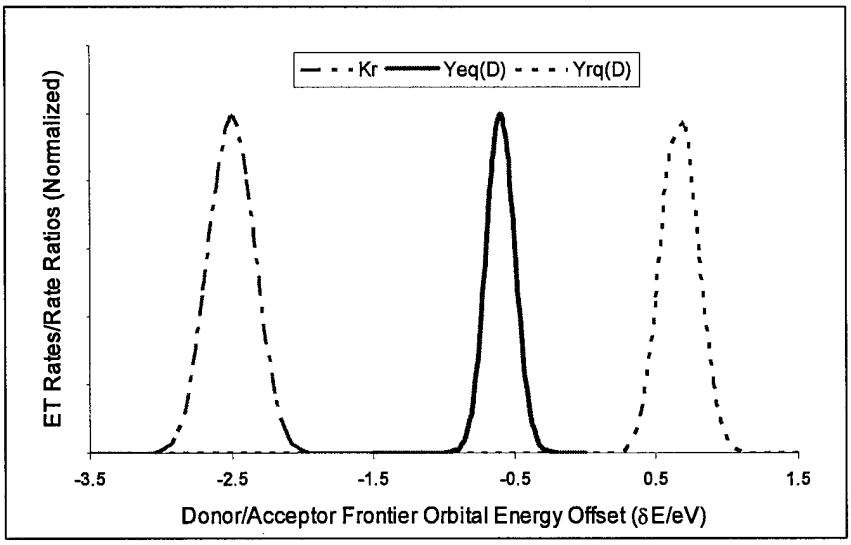

Figure 21. Donor RO-PPV exciton quenching parameter ($Y_{eq(D)}=k_{s(D)}/k_{d(D)}$, middle solid curve), charge recombination rate constant (K_r, left long dashed curve), and charge recombination quenching parameter ($Y_{rq(D)}=k_{s(D)}/k_{r(D)}$, right short dashed curve) versus LUMO offset of RO-PPV/SF-PPV-I pair.

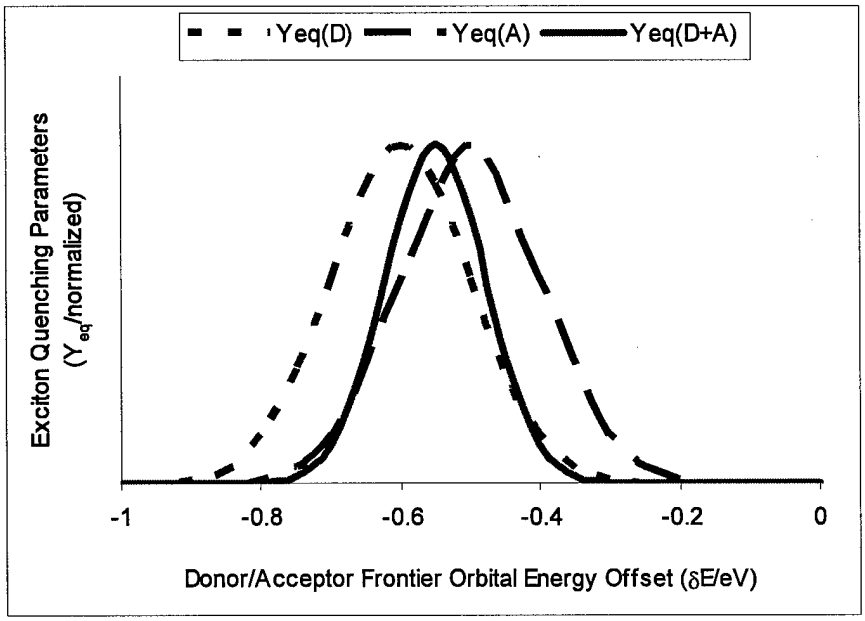

Figure 22. Exciton quenching parameters of the donor RO-PPV (left long dashed curve), acceptor SF-PPV-I (right short dashed curve), and their product $Y_{eq(D)}Y_{eq(A)}$ (middle solid curve) versus the frontier LUMO orbital energy offset.

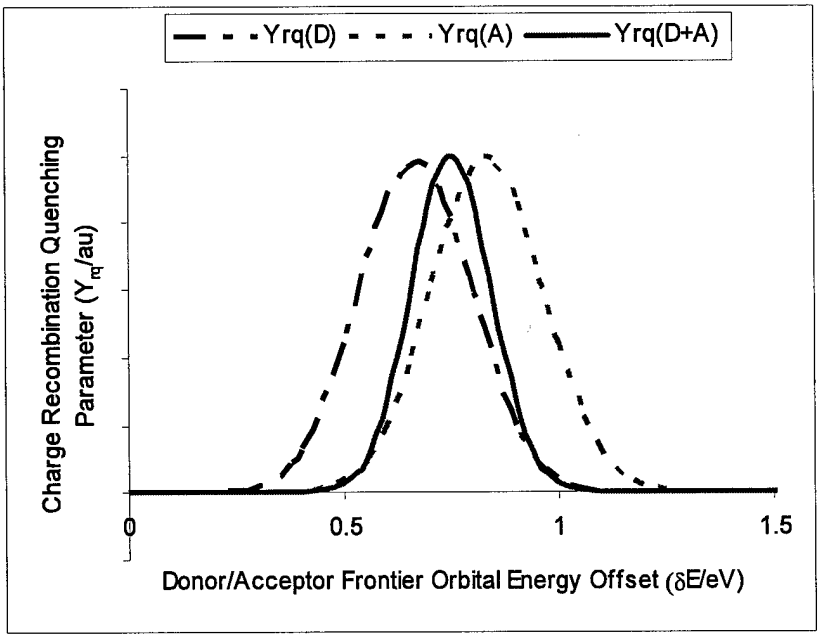

Figure 23. Charge recombination quenching parameters of the donor RO-PPV (left long dashed curve), acceptor SF-PPV-I (right short dashed curve), and their product $Y_{rq(D+A)}=Y_{rq(D)}Y_{rq(A)}$ (middle solid curve) versus the frontier LUMO orbital energy offset.

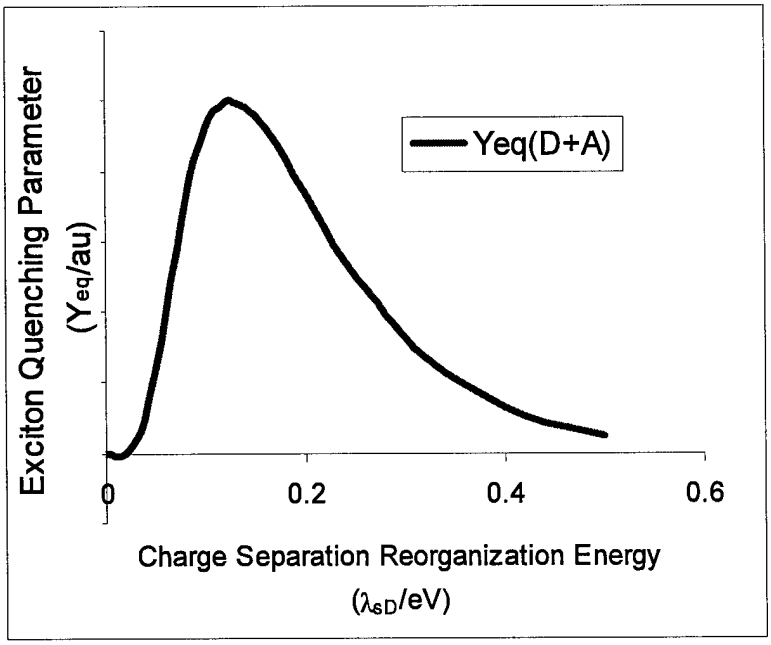

Figure 24. Exciton quenching parameter $Y_{cs(D+A)}$ of RO-PPV/SF-PPV-I pair versus donor RO-PPV charge separation (λ_{sD}) reorganization energy.

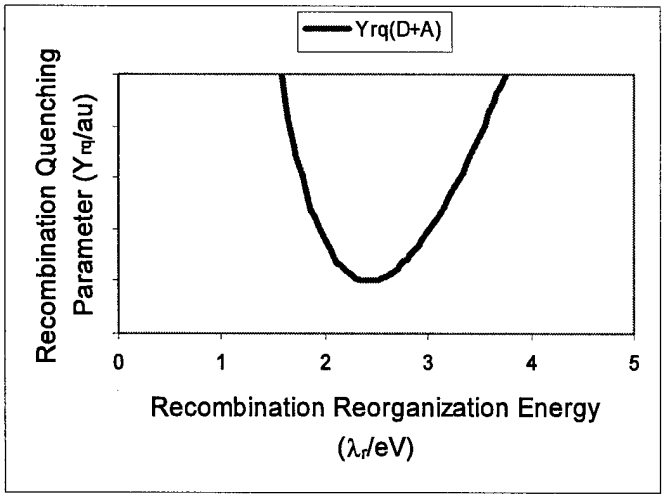

Figure 25. Recombination quenching parameter $Y_{rq(D+A)}$ of RO-PPV/SF-PPV-I pair versus charge recombination reorganization energy of (λ_r).

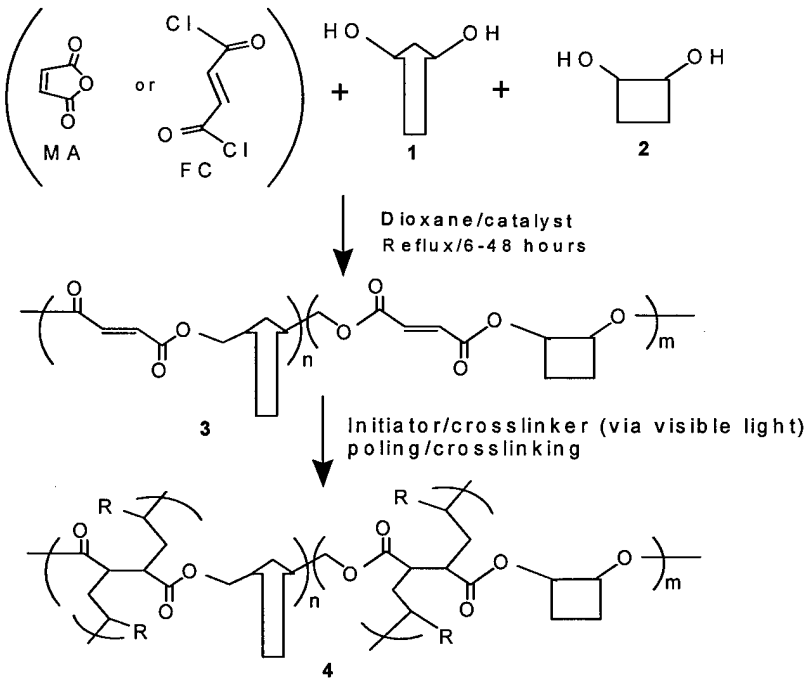

Figure 26. Synthetic and Processing Schemes of Visible Light Crosslinked PDRMA/PDRFC.

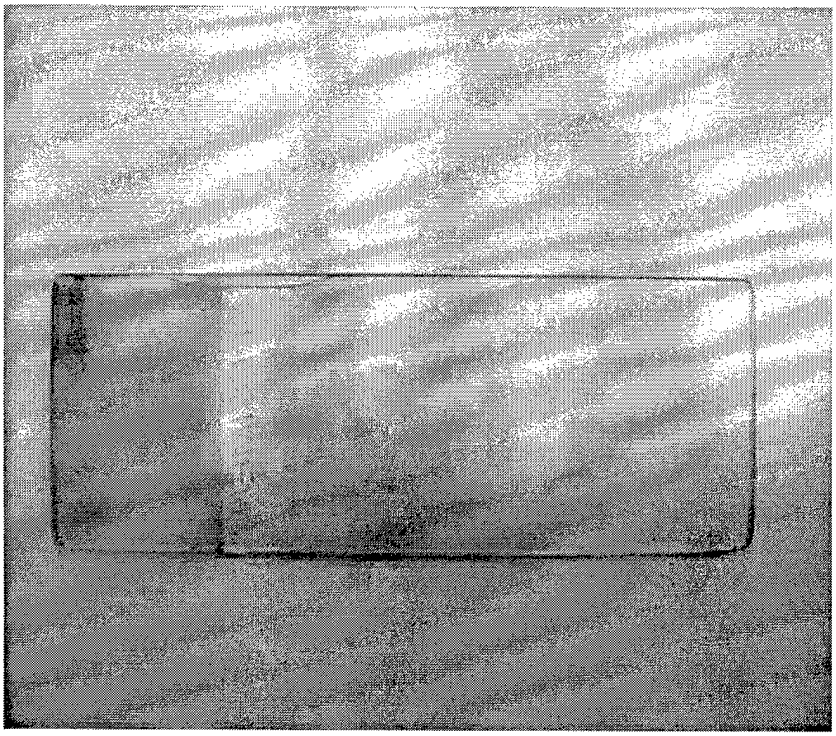

Figure 27. First Thin Film Pattern Fabricated from Visible Light Crosslinking.

5. CITED LITERATURE REFERENCES

[1] M. D. Archer and R. Hill, eds., *Clean Electricity From Photovoltaics*, Imperial College Press, London, UK, 2001.

[2] S. Sun and N. S. Sariciftci, eds., *Organic Photovoltaics: Mechanisms, Materials and Devices*, Marcel Dekker, New York, 2004, in press.

[3] Z. Kafafi and P. Lane, eds., *Organic Photovoltaics IV*, SPIE, Bellingham, 2004.

[4] C. Brabec, V. Dyakonov, J. Parisi, and N. Sariciftci, Organic Photovoltaics: Concepts and Realization, Springer, Berlin, 2003.

[5] A. Hagfeldt and M. Graetzel., *Acct. Chem. Res.*, **33**, 269 (2000).

[6] C. Tang, Two-layer Organic Photovoltaic Cell, *Appl. Phys. Lett.* **48**, 183-185 (1986).

[7] N. S. Sariciftci, L. Smilowitz, A. J. Heeger, F. Wudl, Photoinduced Electron Transfer from a Conducting Polymer to Buckminsterfullerene, *Science*, **258**, 1474 (1992).

[8] B. Kraabel, J. Hummelen, D. Vacar, D. Moses, N. Sariciftci, A. Heeger, F. Wudl, Subpicosecond Photoinduced Electron Transfer From Counjugated Polymers to Functionalized Fullerenes, *J. Chem. Phys.*, **104**, 4267-4273 (1996).

[9] G. Yu, J. Gao, J. Hummelen, F. Wudl, A. Heeger, Polymer Photovoltaic Cells: Enhanced Efficiencies via a Network of Internal Donor-Acceptor Heterojunctions, *Science* **270**,1789-1791 (1995).

[10] L. Schmidt-Mende, A. Fechtenkötter, K. Müllen, E. Moons, R. H. Friend, and J. D. MacKenzie, Self-Organized Discotic Liquid Crystals for High-Efficiency Organic Photovoltaics, *Science*, **293**, 1119 (2001).

[11] M. Granström, K. Petritsch, A. Arias, A. Lux, M. Andersson, R. Friend, Laminated Fabrication of Polymeric Photovoltaic Diodes, *Nature*, **395**, 257-260 (1998).

[12] L. S. Roman, M. Anderson, T. Yohannes and O. Inganas, Photodiode Performance and Nanostructure of Polythiophene/C60 Blends, *Adv. Mater.*, **9**, 1164 (1997).

[13] B. Boer, U. Stalmach, P. Hutten, C. Melzer, V. Krasnikov, G. Hadziioannou, Supramolecular self-assembly and opto-electronic properties of semi conducting block copolymers, *Polymer*, **42**, 9097 (2001).

[14] S. Sun, Design of a Block Copolymer Solar Cell, *Sol. Energy Mat. Sol. Cells*, **79**, 257-264 (2003).

[15] T. A. Skotheim, R. L. Elsenbaumer, J. R. Reynolds, Eds., *Handbook of Conducting Polymers*, 2nd ed., Marcel Dekker, New York, 1998.

[16] J. Perlin, *From Space to Earth-The story of Solar Electricity*, AATEC Publications, Ann Arbor, Michigan, 1999.

[17] M. Knupfer, Exciton Binding Energies in Organic Semiconductors, *Appl. Phys. A*, 77, 623-626 (2003).

[18] T. Stübinger, W. Brütting, Exciton diffusion and optical interference in organic donor–acceptor photovoltaic cells, *J. Appl. Phys.*, **90**, 3632 (2001).

[19] H. Amerongen, L. Valkunas and R. Grondelle, eds., *Photosynthetic Excitons*, World Scientific, Singapore, 2000.

[20] C. Brabec, *et al.*, Origin of the Open Circuit Voltage of Plastic Solar Cells, *Adv. Funct. Mater.*, **11**, 374-380 (2001).

[21] C. Brabec, C., C. Winder, N. Sariciftci, J. Hummelen, A. Dhanabalan, P. Hal, R. Janssen, A Low-Bandgap Seminconducting Polymer for Photovoltaic Devices and Infrared Emitting Diodes, *Adv. Funct. Mater.*, **12**, 709-712 (2002).

[22] N. Sariciftci, *et al.*, Convenient Synthesis and Polymerization of 5,6-Disubstituted Dithiophthalides Toward Soluble Poly(Isothianaphthene): An Initial Spectroscopic Characterization of the Resulting Low-Band-Gap Polymers, *J. Poly. Sci., A.*, **41**, 1034-1045 (2003).

[23] V. Seshadri and G. Sotzing, "Progress in Optically Transparent Conducting Polymers", in *Organic Photovoltaics: Mechanisms, Materials and Devices*, S. Sun and N. S. Sariciftci, eds., Marcel Dekker, New York, 2004, in press.

[24] B. Gregg, Excitonic Solar Cells, *J. Phys. Chem. B.*, **107**, 4688-4698 (2003).

[25] N. Hadjichristidis, S. Pispas, G. Floudas, eds., Block Copolymers: Synthetic Strategies, Physical Properties, and Applications, John Wiley & Sons, Inc., New York, 2003.

[26] M. Lazzari, and M. Lopez-Quintela, Block Copolymers as a Tool for Nanomaterials Fabrication, *Adv. Mater.* **2003**, *15*, 1584-1594.

[27] X. L. Chen and S. A. Jenekhe, Block Conjugated Copolymers: Toward Quantum-Well Nanostructures for Exploring Spatial Confinement Effects on Electronic, Optoelectronic, and Optical Phenomena, *Macromolecules*, **29**, 6189 (1996).

[28] S. Sun, Z. Fan, Y. Wang, C. Taft, J. Haliburton, S. Maaref; Design and Synthesis of Novel Block Copolymers for Efficient Optoelectronic Applications, in "*Organic Photovoltaics II*", *SPIE Proc.*, **4465**, 121 (2002).

[29] Z. Fan, Synthesis and Characterization of A Novel Block Copolymer System Containing RO-PPV And SF-PPV-I Conjugated Blocks, MS Thesis, Norfolk State University, Norfolk, Virginia, July 2002.

[30] S. Sun, Z. Fan, Y. Wang, J. Haliburton, C. Taft, K. Seo, C. Bonner, Conjugated Block Copolymers for Opto-Electronic Functions, *Syn. Met.*, **137**, 883-884 (2003).

[31] S. Sun, Z. Fan, Y. Wang, C. Taft, J. Haliburton, S. Maaref, Synthesis and Characterization of a Novel –DBAB- Block Copolymer System for Potential Light Harvesting Applications, in "*Organic Photovoltaics III*", *SPIE*, **4801**, 114-128 (2003).

[32] S. Sun, Design and Development of Conjugated Block Copolymers for Use in Photovoltaic Devices, in "*Organic Photovoltaics IV", SPIE*, **5215**, 195-205 (2004).

[33] S. Sun, J. Haliburton, Spectroscopic Properties of a Novel –D-B-A-B- Type Block Copolymer and its Component Blocks, to be submitted.

[34] S. Sun, Z. Fan, Y. Wang, J. Haliburton, S. Vick, M. Wang, S. Maaref, K. Winston, A. Ledbetter, and C. E. Bonner, Synthesis and characterization of a –donor-bridge-acceptor-bridge type block copolymer containing poly-p-phenylenevinylene conjugated donor and acceptor blocks, to be submitted.

[35] S. Sun, Z. Fan, Y. Wang, K. Winston, and C. E. Bonner, Morphological Effects to Carrier Mobility in a RO-PPV/SF-PPV Donor/Acceptor Binary Thin Film Opto-electronic Device, *Mater. Sci. Eng. B.*, 2004, in press.

[36] D. Gosztola, B. Wang and M. R. Wasielewski, Factoring through-space and through-bond contributions to rates of photoinduced electron transfer in donor-spacer-acceptor molecules, *J. Photochem. & Photobiol. (A)*, **102**, 71-80 (1996).

[37] D. Adam, P. Schuhmacher, J. Simmerer, L. Haussling, K. Siemensmeyer, K. Etzbach, H. Ringsdorf, D. Haarer, Fast Photoconduction in the Highly Ordered Columnar Phase of a Discotic Liquid Crystal, *Nature*, **371**, 141 (1994).

[38] Z. Bao, A. Dodabalapur, and A. J. Lovinger, Soluble and processable regioregular poly(3-hexylthiophene) for thin film field-effect transistor applications with high mobility, *Appl. Phys. Lett.*, **69**, 4108 (1996).

[39] T. Nguyen, J. Wu, V. Doan, B. Schwartz, S. H. Tolbert, Control of Energy Transfer in Oriented Conjugated Polymer-Mesoporous Silica Composites, *Science*, **288,** 652-656 (2000).
[40] Private communication from Professor Marc Hillmyer.
[41] V. Balzani, ed., *Electron Transfer in Chemistry*, Wiley-VCH, New York, 2000.
[42] R. Marcus, *et al.*, Charge Transfer on the Nanoscale: Current Status, *J. Phys. Chem., B,* **107**, 6668-6697 (2003).
[43] S. Sensfuss, *et al.* Characterization of potential donor acceptor pairs for polymer solar cells by ESR, optical and electrochemical investigations, in *Organic Photovoltaics IV*, Kafafi, Z and Lane, P., eds., *SPIE-proc.*, vol. **5215**, 129-140 (2004).
[44] E. Peeters, P. Hal, J. Knol, C. Brabec, N. Sariciftci, J. Hummelen, R. Janssen, Synthesis, Photophysical Properties, and Photovoltaic Devices of Oligo(p-phenylenevinylene)-fullerene Dyeds, *J. Phy. Chem. B*, **104**, 10174-10190 (2000).
[45] J. Bredas, *et al.*, Alternating Oligo(p-phenylene vinylene)-Perylene Bisimide Copolymers, *J. Am. Chem. Soc.*, **125**, 8625-8638 (2003).
[46] S. Sun, "Optimum Energy Levels for Organic Solar Cells", project briefings to AFOSR and NASA, and *Mater. Sci. & Eng., B*, (2004), in press.
[47] S. Sun, Optimal energy offsets for organic donor/acceptor binary solar cells, *Sol. Energy Mater. Sol. Cells*, (2004), in press.
[48] S. Sun and J. Haliburton, Organic Solar Cell Optimizations, *J. Mater. Sci.*, (2004), in press.
[49] A. Weller, Photoinduced Electron Transfer in Solution, *Z. Phys. Chem.*, **133**, 93-98 (1982).
[50] J. Miller, L. Calcaterra, G. Closs, Intramolecular Long-Distance Electron Transfer in Radical Anions, *J. Am. Chem. Soc.*, **106**, 3047-3049 (1984).

6. PROJECT SUPPORTED PERSONNELS

The project PI, Professor Sam Sun, has been supported with partial teaching release during most of the project period. Two other participating faculty members (Professors C. Bonner and R. Rakhimov) have also been supported partially with a few summer month wages. Although one research faculty (postDoc) and four graduate students were originally budgeted in this project, in reality, more then one participating or collaborating research faculty (*e.g.*, Drs. S. Maaref, C. Zhang, etc.) were supported during the period for their participation and contribution. More than four graduate students and a number of undergraduate students were supported per project needs. Several project participating research students were partially or fully supported by other grants, *e.g.*, from the Department of Education (Title III grant), the NSF (CREST grant), or NASA (University Research Center grant).

7. PROJECT GENERATED PUBLICATIONS

1. Sun, S. and Sariciftci, S., eds., *Organic Photovoltaics: Mechanisms, Materials and Devices*, CRC Press, Boca Raton, Florida, **2005**, ISBN 0-82475-963-X, in production.

2. Sun, S. and Bonner, C., "Chapter 8: Optimizations of Organic Solar Cells in Both Space and Energy/Time Domains", in *Organic Photovoltaics: Mechanisms, Materials and Devices*, edited by Sun and Sariciftci, CRC Press, Boca Raton, Florida, **2005**, in press.
3. Sun, S.; Fan, Z.; Wang, Y.; Haliburton, J., "Organic Solar Cell Optimizations", *J. Mater. Sci.*, **2004**, in press.
4. Sun, S., "Optimal energy levels for organic donor/acceptor binary photovoltaic materials and solar cells", *Mater. Sci. & Eng., B*, **2004**, in press.
5. Sun, S.; Fan, Z.; Wang, Y.; Winston, K. and Bonner, C., "Morphological Effects to Carrier Mobility in a RO-PPV/SF-PPV Donor/Acceptor Binary Thin Film Opto-electronic Device", *Mater. Sci. & Eng. B*, **2004**, in press.
6. Sun, S., "Optimal energy offsets for organic solar cells containing a donor/acceptor pair", *Sol. Energy Mater. Sol. Cells*, **2004**, in press, published online June 20, 2004.
7. Maaref, S.; Thomas, S.; Wang, M. and Sun, S., "New Polythiophene Block Copolymers for Potential Light Harvesting Applications", in *Organic Optoelectronics, SPIE*, **2004**, vol. 5464, pp157-164.
8. Sun, S.; "Design and Development of Conjugated Block Copolymers for Use in Photovoltaic Devices", in *Organic Photovoltaics IV, SPIE*, **2004**, vol. 5215, pp195-205.
9. Sun, S., "Photovoltaic Devices Based on a Novel Block Copolymer", US *patent publication # US 2004/0099307 A1,* published May 27, **2004**.
10. Maaref, S.; Roz, Z.; Sun, S.; Seo, K.; Bonner, C., "Fumaryl Chloride and Maleic Anhydride Derived Crosslinked Functional Polymers for NLO Waveguide Applications", *J. Appl. Poly. Sci.*, **2004**, *92*, 317-322.
11. Sun, S.; Fan, Z.; Wang, Y.; Taft, C.; Haliburton, J.; Maaref, S.; Ledbetter, A.; Bonner, C., "Block Copolymers for Optoelectronics", in *Materials, Active Devices, and Optical Amplifiers, SPIE*, **2004**, vol. 5280, pp253-263.
12. Sun, S., *"Design of a Block Copolymer Solar Cell", Sol. Ener. Mater. Sol. Cel.*, **2003**, *79(2)*, 257.
13. Thomas, S. and Sun, S., "Synthesis and Characterization of a New Polythiophene with Fluorinated Substituents", *Poly. Prepr.*, **2003**, *441(1)*, 891.
14. Roz, Z. and Sun, S., "Synthesis and Characterization of a New Photo Crosslinkable Polyester for Photonic Applications", *Poly. Prepr.*, **2003**, *441(1)*, 86.
15. Haliburton, J. and Sun, S., "Design and Synthesis of a New Fluorinated Polyphenylenevinylene 'SF-PPV-II'", *Poly. Prepr.*, **2003**, *441(1)*, 890.
16. Maaref, S and Sun, S., "New Terminal Functionalized Polythiophenes with Size Control", *PMSE*, **2003**, *88*, 510.
17. Sun, S., "Block Copolymers for Photovoltaics", *PMSE*, **2003**, *88*, 158.
18. Sun, S.; Fan, Z.; Wang, Y.; Taft, C.; Haliburton, J.; Maaref, S.; "Synthesis and Characterization of a Novel –D-B-A-B- Block Copolymer System for Light Harvesting Applications", in *Organic Photovoltaics III, SPIE*, **2003**, vol. 4801, pp114-124.
19. Sun, S.; Fan, Z.; Wang, Y.; Haliburton, J.; Taft, C.; Seo, K.; Bonner, C., "Conjugated Block Copolymers for Opto-Electronic Functions", *Syn. Met.*, **2003**, *137(1-3)*, 883-884.

20. Maaref, S.; Roz, Z.; Sun, S.; Barto, R.; Frank, C., "Photocrosslinking and SHG Stability of PDRMA/PDRFC Thin Films", *SPIE*, **2002**, vol. 4798, pp203-211.
21. Ma, J.; Song, H.; Frisch, H. L; Maaref, S.; Sun, S., "Electrically Conductive Semi-IPNs Based on Polyaniline and Crosslinked Polyvinylacetate", *J. Appl. Poly. Sci.*, **2002**, *85(11)*, 2287-2293.
22. Sun, S.; Maaref, S.; Bonner, C., "Chapter 2: Fumaryl Chloride and Maleic Anhydride Derived Crosslinked Functional Polymers and Nano Structures", in *Functional Condensation Polymers*, eds., C. Carraher and G. Swift, Kluwer Academic Press, New York, **2002**, pp 17-30.
23. Fan, Z.; Wang, Y.; Taft, C.; Haliburton, J.; Maaref, S. and Sun, S., "Synthesis and Characterization of a novel block copolymer containing donor and acceptor blocks", *PMSE,* **2002,** *86,* 47.
24. Wang, Y. and Sun, S., "Synthesis and Characterization of SF-PPV I", *PMSE*, **2002**, *86*, 67.
25. Sun, S.; Maaref, S.; Alam, E., Wang, Y.; Fan, Z.; Bahoura, M.; Higgins, P.; Bonner, C. "Recent Development of Crosslinked NLO Polymers for Large Bandwidth Electro-Optical Modulations", *SPIE*, **2001**, vol. 4580, pp 297-308.
26. Sun, S.; Fan, Z.; Wang, Y.; Taft, C.; Haliburton, J.; Maaref, S.; "Design and Synthesis of Novel Block Copolymers for Efficient Opto-Electronic Applications", in *Organic Photovoltaics II, SPIE*, **2002**, vol. 4465, pp 121-128.
27. Seo, K.; Bonner, C.; Maaref, S.; Sun, S.; "Dielectric and Nonlinear Optical Properties of Fumaryl Type Photo Crosslinkable Polyesters", in *Quantum Confinement: Nano Structured Materials and Devices*, ECS, **2001**, pp 358-365.
28. Sun, S.; Maaref, S.; Alam, E.; Wang, Y.; Bahoura, M.; Bonner, C., "Synthesis and Characterization of Fumaryl Chloride Type Functional Crosslinked Polyesters", *PMSE*, **2001**, *84*, 431.

8. PROJECT GENERATED PRESENTATIONS/LECTURES

1. Sun, S., "Optimizations of Organic Solar Cells", presentation at the 228th ACS National Meeting, Philadelphia, PA, August, **2004**.
2. Sun, S., *et al.*, "Conjugated Block Copolymers for Photovoltaics: Optimization of Photoelectric Efficiency in Both Space and Energy/Time Domains", presentation at the 2nd IECEC International Conference, Providence, RI, August, **2004**.
3. Sun, S, "Polymer morphology and energy levels versus photoelectric power conversion efficiencies: a preliminary account", presentation at SPIE 49th Annual meeting, Denver, Colorado, August, **2004**.
4. Sun, S.; *et al.*, "Center for Research and Education in Advanced Materials", presentation at NASA HBCU/MI 2004 Conference, Cleveland, OH, July, **2004**.
5. Sun, S. and Bonner, C., "Optimizing organic solar cells in both space and energy domains", presentation at ICSM-2004 Conference, Wollongong, Australia, June, **2004**.
6. Sun, S.; "Optimization of Organic Solar Cells", presentation at SCELL-2004, Badjoz, Spain, May, **2004**.
7. Sun, S, *et al.*, "Block Copolymers for Photovoltaics", presentation at SPIE Photonic-Europe Conference, Strausburg, France, April, **2004**.

8. Sun, S., "Improving Opto-electronic Efficiency via Bridged Donor and Acceptor Block Copolymers", presentation at the 227th ACS National Meeting, Anaheim, CA, March, **2004**.
9. Sun, S. "Block Copolymers for Photovoltaics: Toward Plastic Solar Cells", an invited seminar presentation at California State University, Northridge, California, March 29, **2004**.
10. Sun, S. "Block Copolymers for Photovoltaics: Toward Plastic Solar Cells", an invited seminar presentation at Vanderbilt University, Nashville, Tennessee, February 25, **2004**.
11. Sun, S. "Self-assembled Macromolecules for Sun Light Harvesting", an invited seminar presentation at Peking University, Beijing, China, November 11, **2003**.
12. Sun, S. "Block Copolymers for Photovoltaics: Toward Plastic Solar Cells", an invited seminar presentation at East China University of Science and Technology, Shanghai, China, November 6, **2003**.
13. Sun, S.; Fan, Z.; Wang, Y.; Taft, C.; Haliburton, J.; Maaref, S.; Ledbetter, A.; Bonner, C., "Block Copolymers for Optoelectronics", presentation at SPIE-APOC-2003 Conference, Wuhan, China, November, **2003**.
14. Sun, S.; "Design and Development of Conjugated Block Copolymers for Use in Photovoltaic Devices", presentation at SPIE 2003 Annual Convention, San Diego, California, August, **2003**.
15. Sun, S. "Toward Plastic Solar Cells", an invited seminar presentation at Chemistry department at University of Southern California (USC), Los Angeles, USA, August 1, **2003**.
16. Sun, S.; Fan, Z.; Wang, Y.; Haliburton, J.; Taft, C.; Seo, K.; Bonner, C., "Conjugated Block Copolymers for Opto-Electronic Functions", presentation at the International Conference on Synthetic Metals 'ICSM2002' at Shanghai, China, June, **2002**.
17. Maaref, S.; Roz, Z.; Sun, S.; Barto, R.; Frank, C., "Photocrosslinking and SHG Stability of PDRMA/PDRFC Thin Films", presentation at SPIE 2002 Annual Convention, Seattle, Washington, July, **2002**.
18. Sun, S., "Organic and Polymeric Electro-active Materials", an invited lecture at a joint chemistry/physics departmental seminar at Hampton University, Virginia, USA, April 4, **2002**.
19. Sun, S.; Maaref, S.; Alam, E., Wang, Y.; Fan, Z.; Bahoura, M.; Higgins, P.; Bonner, C. "Recent Development of Crosslinked NLO Polymers for Large Bandwidth Electro-Optical Modulations", presentation at the International SPIE/APOC-2001 Conference, Beijing, China, November, **2001**.
20. Sun, S., "Electro-Active Functional Polymers", invited seminar presentation at both physics and polymer departments at Peking University, Beijing, China, November, **2001**.
21. Sun, S.; Fan, Z.; Wang, Y.; Taft, C.; Haliburton, J.; Maaref, S.; "Design and Synthesis of Novel Block Copolymers for Efficient Opto-Electronic Applications", presentation at SPIE 2001 Annual Convention, San Diego, California, July, **2001**.
22. Sun, S.; Maaref, S.; Alam, E.; Wang, Y.; Bahoura, M.; Bonner, C., "Synthesis and Characterization of Fumaryl Chloride Type Functional Crosslinked Polyesters",

presentation at ACS 2001 Spring National Convention and Exhibit, San Diego, March, **2001**.

9. PROJECT GENERATED INVENTIONS/PATENT DISCLOSURES:

Sun, S., "Photovoltaic Devices Based on a Novel Block Copolymer", US *patent publication # US 2004/0099307 A1,* filed November **2002**, published May 27, **2004**.

10. PROJECT GENERATED OR RELATED THESIS

1. Z. Fan, "Synthesis and Characterization of A Novel Block Copolymer System Containing RO-PPV And SF-PPV-I Conjugated Blocks", MS Thesis, Norfolk State University, Norfolk, Virginia, July 2002.
2. Y. Wang, "Synthesis and Characterization of A New Acceptor (N-Type) Conjugated Polymer "SF-PPV-I", MS Thesis, Norfolk State University, Norfolk, Virginia, July 2002.
3. Z. Roz, "Synthesis and Characterization of a New Photocrosslinkable and Processable Polymer for Potential Nonlinear Optical Applications", MS Thesis, Norfolk State University, Norfolk, Virginia, August 2004.
4. J. Haliburton, "Design and Synthesis of New (n-type) Sulfone Derivatized Polyphenylenevinylene (PPV) Acceptor Blocks for Opto-electronic Applications", MS Thesis, Norfolk State University, Norfolk, Virginia, August 2004.
5. S. Thomas, "Synthesis and Characterization of a new Acceptor (N-Type) Fluorinated and Terminal-Functionalized Polythiophene", MS Thesis, Norfolk State University, Norfolk, Virginia, August 2004.

11. HONORS/AWARDS

During the project period (2001-2004), the PI (Professor Sun) received several awards and honors at Norfolk State University. These include "Outstanding Mentoring" and "Outstanding Grantsmanship", "Outstanding Scholarly Activities", etc., which were awarded at NSU's School of Science and Technology Annual Awards Lunch/Banquet.

APPENDIX: MATERIALS SYNTHESIS DETAILS

A-1. General Information

All starting materials, reagents and solvents were purchased from commercial sources (mostly from Sigma-Aldrich) and used directly except noted otherwise. NMR data were obtained from a Bruker Avance 300 MHz spectrometer (TMS as reference). Elemental Analysis was done by Atlantic Microlab Inc. Polymer molecular weight analyses were done using a Viscotek T60A/LR40 triple-detector GPC system with mobile phase of THF at ambient temperature (Universal calibration with polystyrene as standard). UV-VIS spectra were collected using a Varian Gary-5 spectrophotometer. Luminescence spectra were obtained from an ISA Fluoromax-3 luminescence spectrophotometer. For the spectroscopic measurement of polymer solutions, methylene chloride was used as the standard solvent. FT-IR data were obtained from a Nicolet Avatar or Bruker IFS-66 IR spectrometer. Polymer films were prepared from spin coating or drop drying via 0.2 micron filtered methylene chloride polymer solutions on the pre-treated glass slides, and the films were typically dried overnight in heated vacuum oven before any analysis. The thermal analysis was done on a Perkin-Elmer TGA6/DSC6/TMA7 system. The electrochemical data was obtained from a Bioanalytical (BAS) Epsilon100 CV system. In CV measurements, the concentration of polymer solutions (in methylene chloride) were typically 2mM, and the salt $(Bu)_4NPF_6$ concentration was 0.1M. Reference electrode was a standard Silver electrode. The CV scan rate was 100mV/s.

For the final –DBAB- block copolymer, a general synthetic scheme for the synthesis of the polymers (Figure A-1) is as follows: In scheme (a), one molar quantity of acceptor block [A] were added slowly and drop wisely into access amount (more than two molar quantity) of bridge blocks [B] in a polar aprotic solvent (such as dichloromethane) under reflux to yield B-A-B. In the next step, B-A-B was reacted with about equal amount of donor (D) block yielding final donor/acceptor block copolymers.

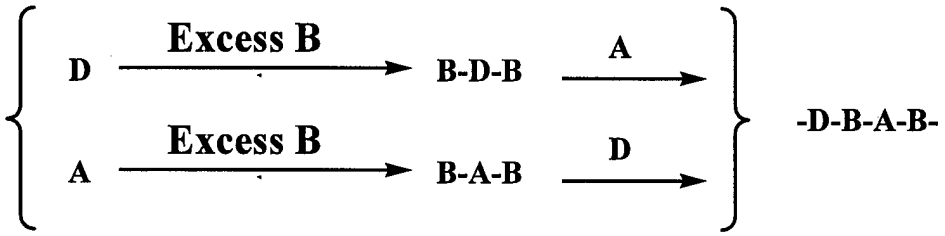

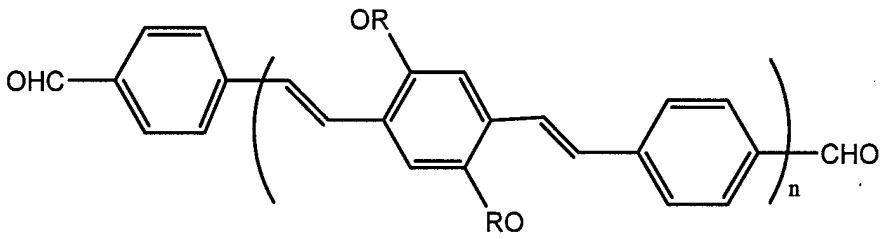

D = Donor Block

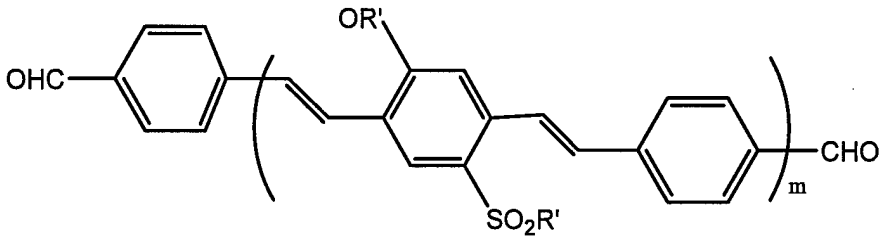

A = Acceptor Block

$R = C_{10}H_{21}$, $R' = C_2H_5$

$H_2N\text{-}(CH_2)_p\text{-}NH_2$

Bridge Unit

Figure A-1. Synthetic Scheme of the block copolymers.

A-2 Donor Block Synthesis

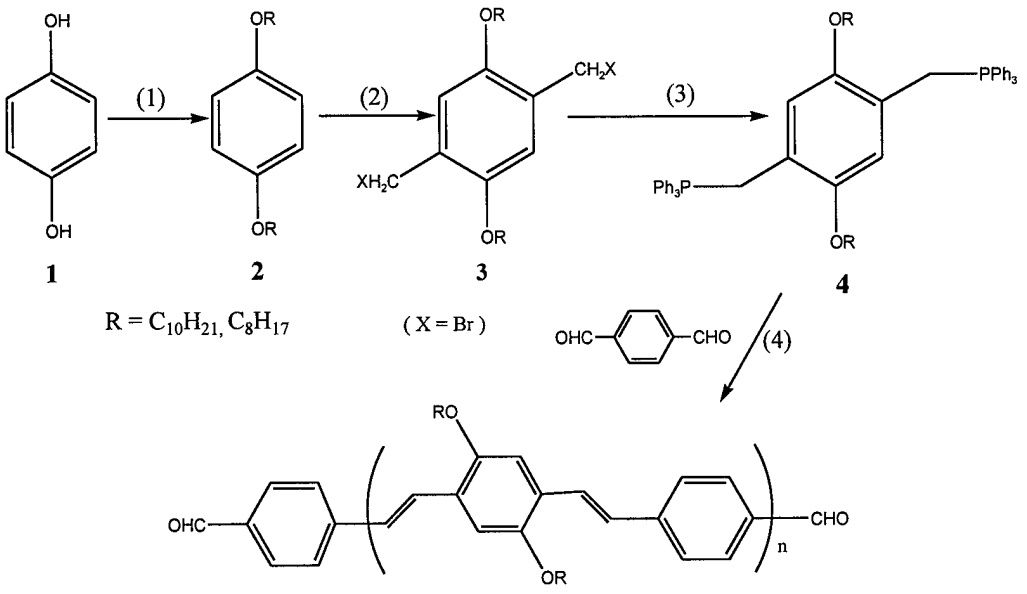

5, Donor Block (D)

Figure A-2. Synthetic Scheme of a Donor Block.

In the synthesis of donor block, both C_8H_{17} and $C_{10}H_{21}$ were used. The reaction conditions and scheme are similar. Different lengths of the side chain were proved to affect little of donor block's opto-electronic properties. It will only affect the physical properties of the monomers and donor block, such as the thermal and solubility properties. Below show is the detailed procedure to synthesis the donor block with $C_{10}H_{21}$ side chain.

Step (1) Synthesis of 1,4-Bis(decyloxy) benzene (compound 2).

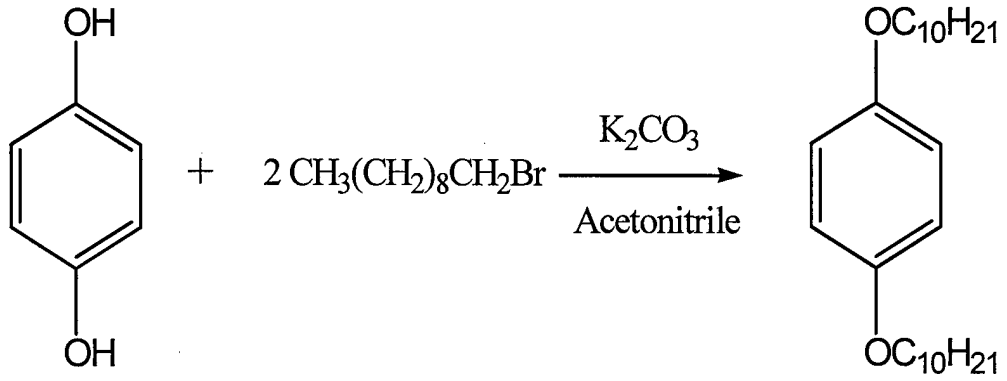

1 **2**

This reaction is a typical Williamson ether synthesis reaction. A suspension of 1,4-hydroquinone **1** (27.5 g, 250 mmol), 1-bromodecane (155ml, 750 mmol), and K_2CO_3 (104.0 g, 750 mmol) in acetonitrile (500 ml) was heated at reflux for two days before being poured into water (600 ml). The precipitates were first collected by filtration and the dissolved in a minimum of hot hexane. Subsequently, the resulting hot solution was poured into methanol (600 ml) to precipitate the product. The precipitates were filtered off and dissolved in hot hexane (200 ml) again. Reprecipitation of resulting solution in methanol then gave 83.0 g pure product **2** as a white solid after filtered and dried under vacuum (85% yield). Melting Point (m.p.) is 65~68° C. ^{1}H NMR ($CDCl_3$) δ (ppm) 0.88 (t, J – 6.86 Hz, 6H, CH_3), 1.27 (m, 12H, $OCH_2CH_2CH_2(CH_2)_6CH_3$), 1.45 (m, 4H, $OCH_2CH_2CH_2(CH_2)_6CH_3$), 1.78 (quintet, 4H, J = 8.14 Hz, $OCH_2CH_2CH_2(CH_2)_6CH_3$), 3.85 (t, J = 6.40 Hz, 4H, $OCH_2CH_2CH_2(CH_2)_6CH_3$), 6.82 (s, 4H, aromatic).

Notes:

In this step, excess amount of 1-bromodecane and K_2CO_3 were used to the reaction moves forward more quickly and all the 1,4-hydroquinone was reacted. The excess 1-bromodecane and potassium hydroxide can be get rid of by pouring the reaction solution into the water, since both of them are well dissolved in water.

The color of the reaction solution changes from bright yellow to brown, then to black at the end of reaction. The reaction process was monitored by TLC (Thin Layer Chromatography, a mixture of Hexane and Ethyl Acetate with ratio 2 to 1 as solvent) to ensure the reaction is complete.

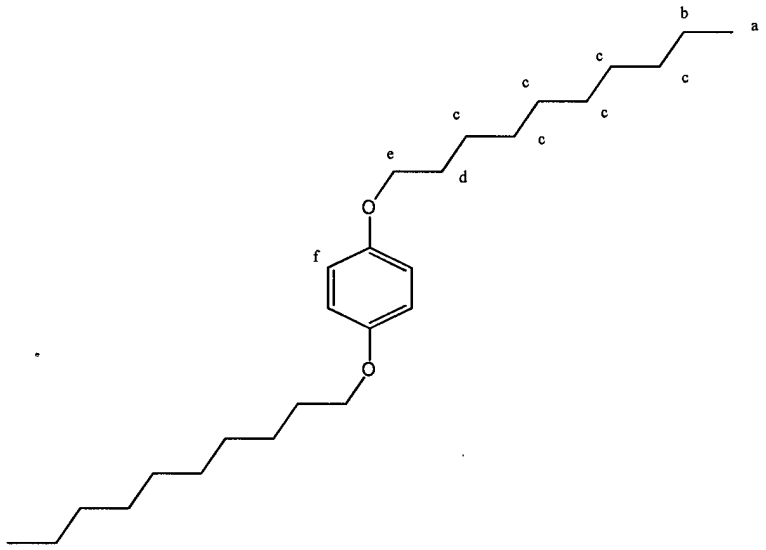

***Structure of* 1,4-Bis(decyloxy) benzene, compound 2**

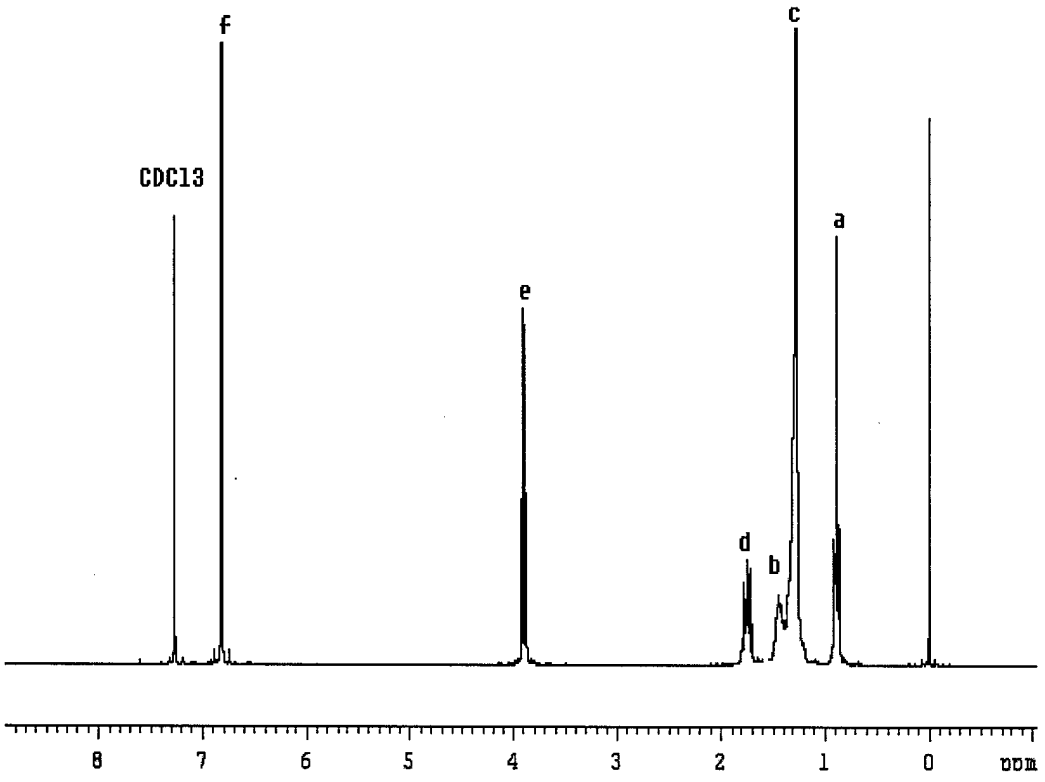

Figure A-3. ^{1}H NMR spectra of compound **2** (1,4-Bis(decyloxy) Benzene).

Step (2) Synthesis of 2,5-Bis(bromomethyl)-1,4-bis(decyloxy)benzene (compound 3).

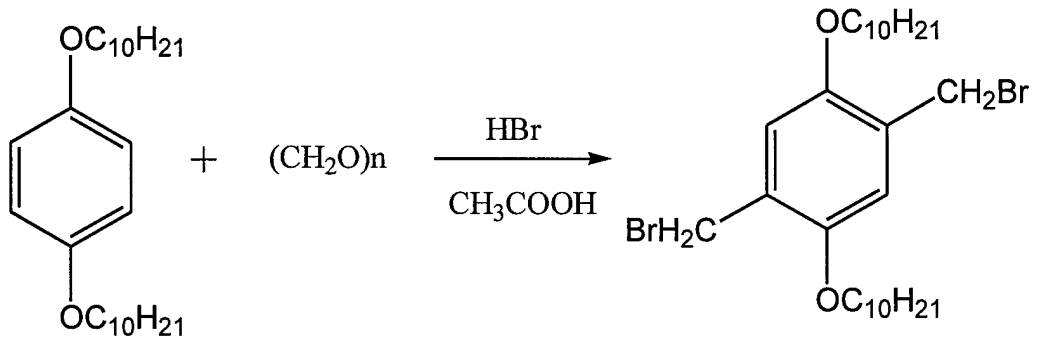

2 **3**

To a suspension of **2** (5.9 g, 15.1 mmol) and paraformaldehyde (0.93 g, 31.0 mmol) in acetic acid (50 ml) was added HBr (6.0 ml, 31 wt % in acetic acid) all at once. This mixture was then heated to 60-70 °C with stirring for 2 h. as the reaction proceeded; the suspension changed to clear solution first and then became a thick suspension again. After cooling to room temperature, this suspension was poured into water (300 ml). The precipitates were filtered and dissolved in hot chloroform. Re-precipitation of the resulting solution in methanol then gave **3** (7.5 g, 86.1 % yield) as a white, loose solid after being filtered and dried under vacuum. Melting Point (m.p.) is 70 ° C ~ 72 ° C. ^{1}H NMR ($CDCl_3$) δ (ppm) 0.88 (t, J – 6.86 Hz, 6H, CH_3), 1.27 (m, 12H, $OCH_2CH_2CH_2(CH_2)_6CH_3$), 1.49 (m, 4H, $OCH_2CH_2CH_2(CH_2)_6CH_3$), 1.81 (quintet, 4H, J = 8.14 Hz, $OCH_2CH_2CH_2(CH_2)_6CH_3$), 3.98 (t, J = 6.40 Hz, 4H, $OCH_2CH_2CH_2(CH_2)_6CH_3$), 4.52 (s, 4H, CH_2Br), 6.82 (s, 2H, aromatic).

Notes:

Unlike the first step reaction, in this step, we cannot use adding more paraformaldehyde to make the reaction goes faster. The ratio of paraformaldehyde to 1,4-Bis(decyloxy) benzene is the key factor to control the final products structure. If the ratio

is higher than 2.3, then both di and tri substitution may be produced at the end of reaction. That means in addition to the compound **3**, a side product with three bromomethyl groups on the benzene ring will be generated. Since compound **3** has similar structure with that of the side product, it is hard to separate them. Therefore, the only way to avoid this side product is to strictly control the ratio of paraformaldehyde and 1,4-bis(decyloxy) benzene to 2.0 to 2.1.

Also, TLC was used to monitor the process of the reaction to ensure the completion of the reaction.

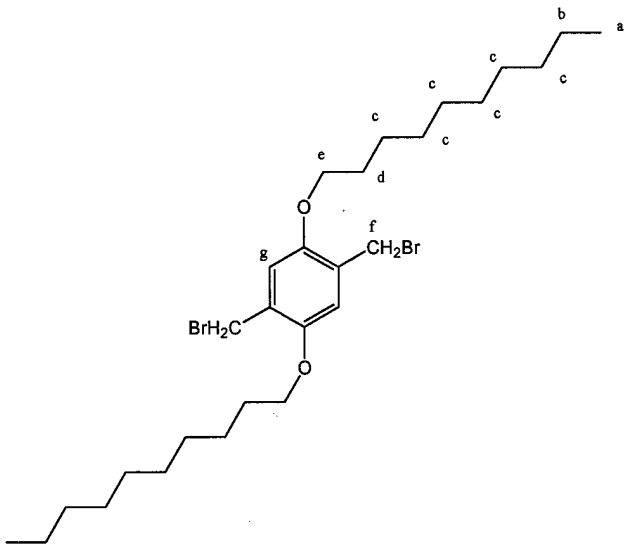

Structure of 2,5-Bis(bromomethyl)-1,4-bis(decyloxy)benzene (compound 3).

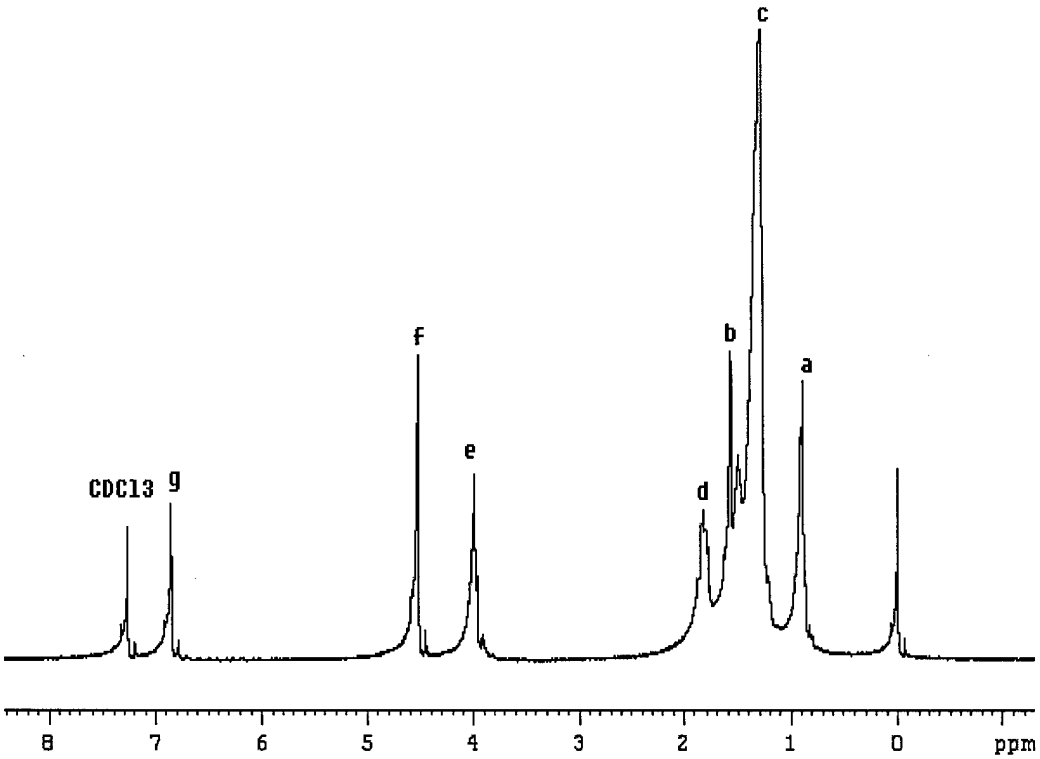

Figure A-4. ^{1}H NMR spectra of compound **3**.

Step 3 Synthesis of 2,5-bis(decyloxy)-1,4-bis(triphenyl phosphite) benzene.

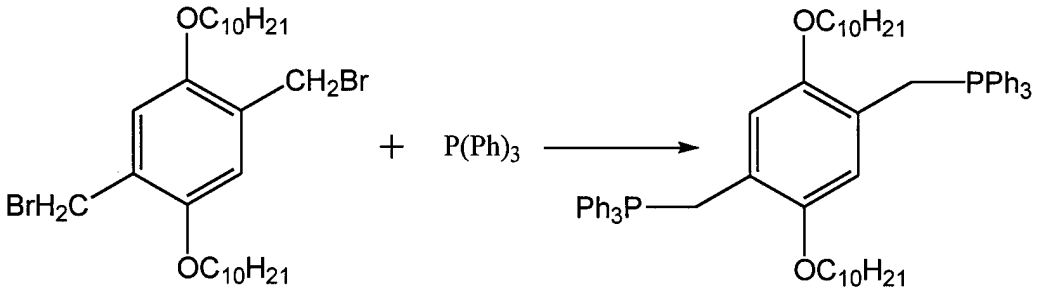

3 **4**

A suspension of compound **3** (0.576 g, 1.0 mmol) and triphenylphosphine (0.550 g, 2.1 mmol) in toluene was heated at reflux for 3 h. The solvent was then removed from the resulting clear solution under reduced pressure. The resulting residue (compound **4**) was then purified by passing through a Gel Chromatography Column. Melting point

(m.p.) is 77 ° C ~ 79 ° C. ^{1}H NMR ($CDCl_3$) δ (ppm) 0.88 (t, J – 6.86 Hz, 6H, CH_3), 1.27 (m, 12H, $OCH_2CH_2CH_2(CH_2)_6CH_3$), 1.49 (m, 4H, $OCH_2CH_2CH_2(CH_2)_6CH_3$), 1.81 (quintet, 4H, J = 8.14 Hz, $OCH_2CH_2CH_2(CH_2)_6CH_3$), 2.98 (t, J = 6.40 Hz, 4H, $OCH_2CH_2CH_2(CH_2)_6CH_3$), 5.31 (s, 4H, CH_2PPh_3), 6.82 (s, 2H, aromatic), 7.75 (m, 30H, PPh_3). Elemental analysis result is: C 70.52%, H 6.44%, O 3.56%, calculated: C 69.81%, H 7.14%, O 2.91%. Also, high resolution mass of compound 4 with two di ethoxy phosphate groups shows a peak at 690.7, which is almost the same with calculated molecular weight (690.8).

Notes:

In Step (3) to synthesize compound 4, excess amount of tri-phenyl phosphite was used to expedite the reaction. The extra tri-phenyl phosphite can be get rid of by washing the final solid with methanol.

The monomer, compound 4, was purified by passing it through the gel chromatography column; the solvent used to pass the column is the mixture of hexane and ethylacetate with ratio 1 to 2. The purified final monomer, compound 4, was characterized by elemental analysis, the result is nearly the same as the predicted one. When passing the compound 4 through the Gel Chromatography Column, 200 mesh gel was used, and the solvent is the mixture of Hexane and Ethyl Acetate with ratio 2 to 1.

In addition to the monomer, compound **4**, with two tri-phenyl phosphite groups on the benzene ring, we also successfully synthesized monomer with two di-ethoxy phosphate groups. The procedure is similar. And since the tri ethoxy phosphite used to do the reaction is a liquid and the boiling point is very low, so no solvent is necessary to do the reaction. This is so called neat reaction and will make it easier to purify the product. . ^{1}H NMR ($CDCl_3$) δ (ppm) 0.88 (t, J – 6.86 Hz, 6H, CH_3), 1.27 (m, 18H, $OCH_2CH_2CH_2(CH_2)_6CH_3$, $PO(OCH_2CH_3)$), 1.49 (m, 4H, $OCH_2CH_2CH_2(CH_2)_6CH_3$), 1.81 (quintet, 4H, J = 8.14 Hz, $OCH_2CH_2CH_2(CH_2)_6CH_3$), 3.23 (d, J = 6.40 Hz, 4H, $OCH_2CH_2CH_2(CH_2)_6CH_3$), 3.85 (d, 8H, $PO(OCH_2CH_3)$), 4.05 (m, 4H, $CH_2PO(OEt_3)$), 6.82 (s, 2H, aromatic).

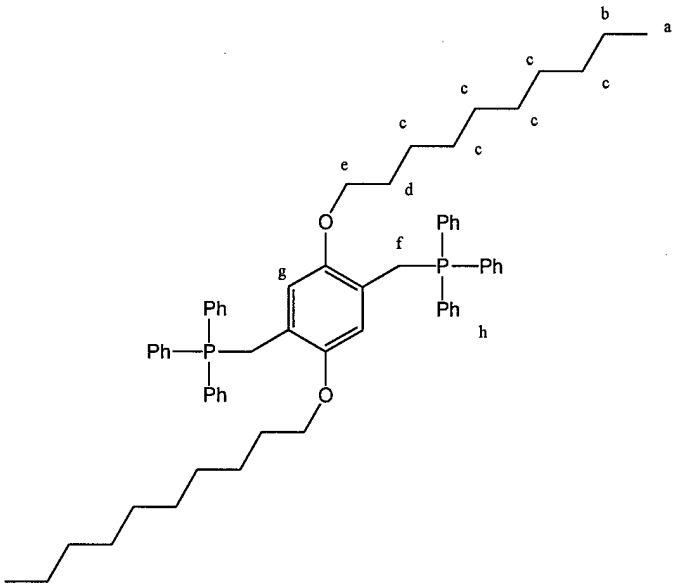

Structure of the Monomer, compound **4**

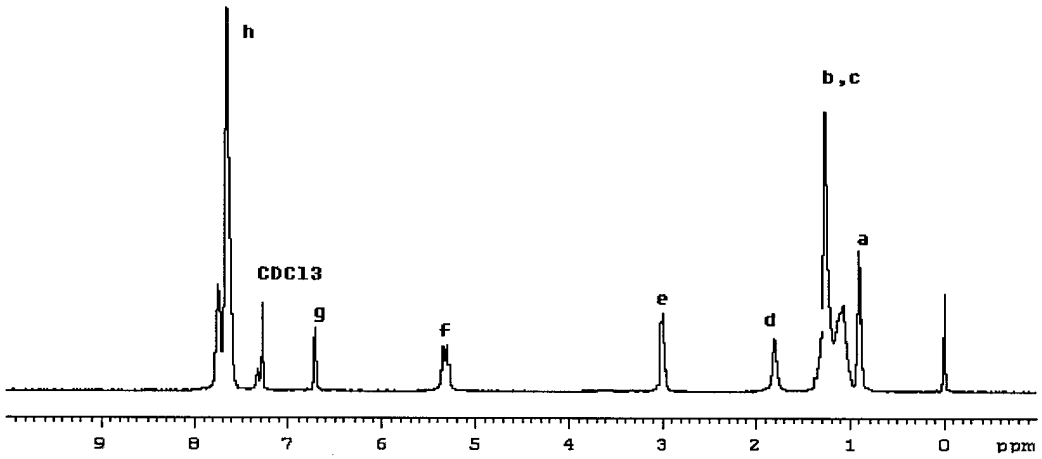

Figure A-5. ^{1}H NMR Spectrum of Compound **4.**

Step 4 Synthesis of 2,5-Bis(decyloxy)-1,4-bis[4-formyl-phenylenevinylene] benzene (donor block 5).

The resulting residue, compound **4** (0.692 g, 1.0 mmol), along with 1,4-benzenedicarboxylaldehyde (0.148 g, 1.1 mmol), was dissolved in methylene chloride (50 ml). To this solution was added lithium ethoxide solution (4.5 ml, 1.0 M in ethanol) drop wise via a syringe at room temperature. The base should be introduced at such a rate that the transient red-purple color produced upon the addition of base should not persist. The resulting solution was allowed to stir for 12 h more after the completion of base addition. This solution was then poured into a mixture solvent of dilute aqueous HCl and methanol, adjust the PH to about 7. The precipitate was separated, washed with water, and dried under vacuum. This afforded 0.66 g of monomer, donor block **5** as a red fluorescent solid. The T_g of a donor block with 3 repeat units is about 68°C.

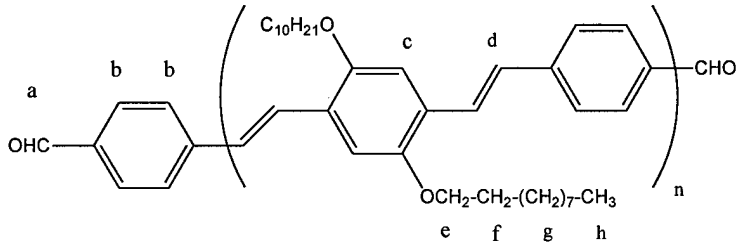

Structure of Donor Block 5

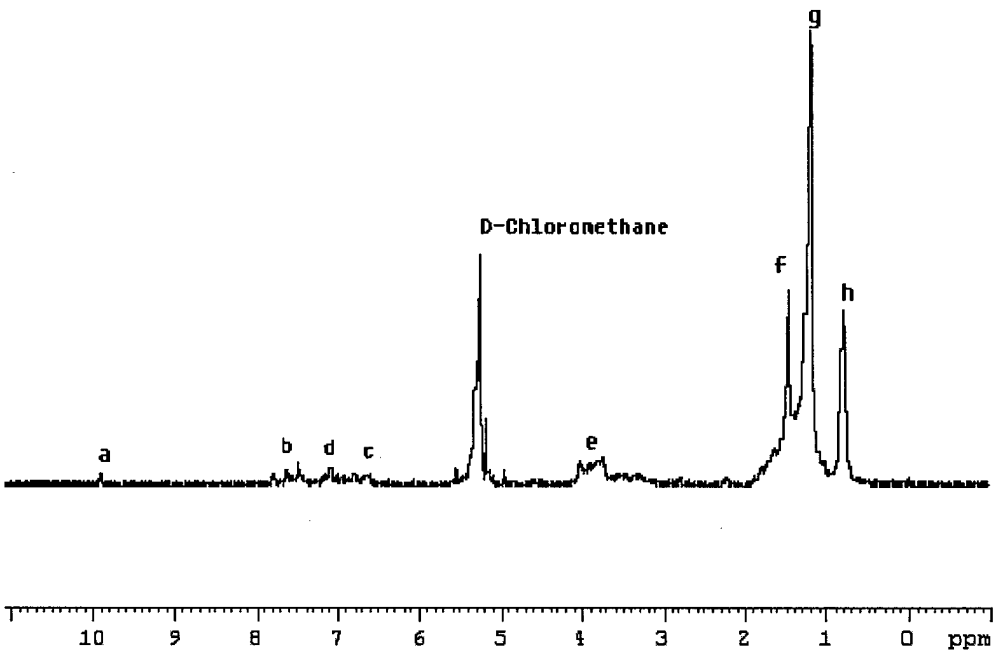

Figure A-6. ^{1}H NMR Spectrum of **5** (Donor Block).

Notes:

In Step 4 to synthesize the Donor Block, the final polymer was characterized by both GPC and MALDI, and both give results of a few thousands molecular weight. The MALDI data also show the distribution of the molecular weight that will be discussed later.

In the synthesis of the Donor Block, we have tried different reaction conditions to control the donor block's molecular weight, thus in this way, we can control the length of the donor block. In general, we use two ways to control the donor block's molecular weight:

The first way is to control the two reactants ratio of Step 4. Since the two reactants of Step 4 have two function groups, in theory, if the ratio of the two reactants is 1:1, the reaction will stop until it is large enough to precipitate out. But if the ratio of two reactants is not 1:1, the reaction will automatically stop at the certain stage with the final molecule ending with the excess function group. For instance, the two reactants we used in step 4 to form the donor block are 2, 5-Bis[triphenyl phosphate]-1, 4-Bis(decyloxy)

benzene and 1,4-dialdyhyde benzene, if we use excess amount of 1,4-dialdyhyde benzene in the reaction, then at the certain time when the molecule grew to certain length, all the triphenyl phosphate were used up and the reaction will stop leaving the donor block ending with two aldehyde groups.

The second way is to use 1:1 monomer ratio but with different reaction conditions to control the block size growth and quench the reaction with a terminating monomer containing desired end groups. GPC can be used to monitor the reaction progress. For instance, when the donor block grew to the desired molecular weight, then add some more 2, 5-Bis[triphenyl phosphate]-1, 4-Bis(decyloxy) benzene or 1,4-dialdyhyde benzene to terminated the reaction. The reaction conditions we can use to control the reaction are reaction temperature, reaction time, the solvent used to do the reaction and the base to initialize the reaction. Normally, the higher the reaction temperature is, the faster the reaction goes. Also, different solvent and base will affect the reaction speed.

Table A-1 lists some reaction conditions we used to control the reaction, and the molecular weight, donor block length and the average number of repeat unit in the block (C_{10} substituted) we got via the reaction condition control.

Reaction ID	Reaction Condition (monomer **4**: 1,4-dialdyhybenzene)	Mw (Dalton, via GPC)	Average # of repeat units	Average Size (nm)	PD
	30°C for 24 hours (1:1.10)	2250	4	4.8	2.2
	30°C for 24 hours (1:1.05)	3300	6	7.2	2.7
	80°C for 24 hours (1:1.05) (DMF as Solvent)	6500	12	14.4	2.9

Table A-1. Donor Block Size versus Synthetic Condition.

A-3 Acceptor Block Synthesis

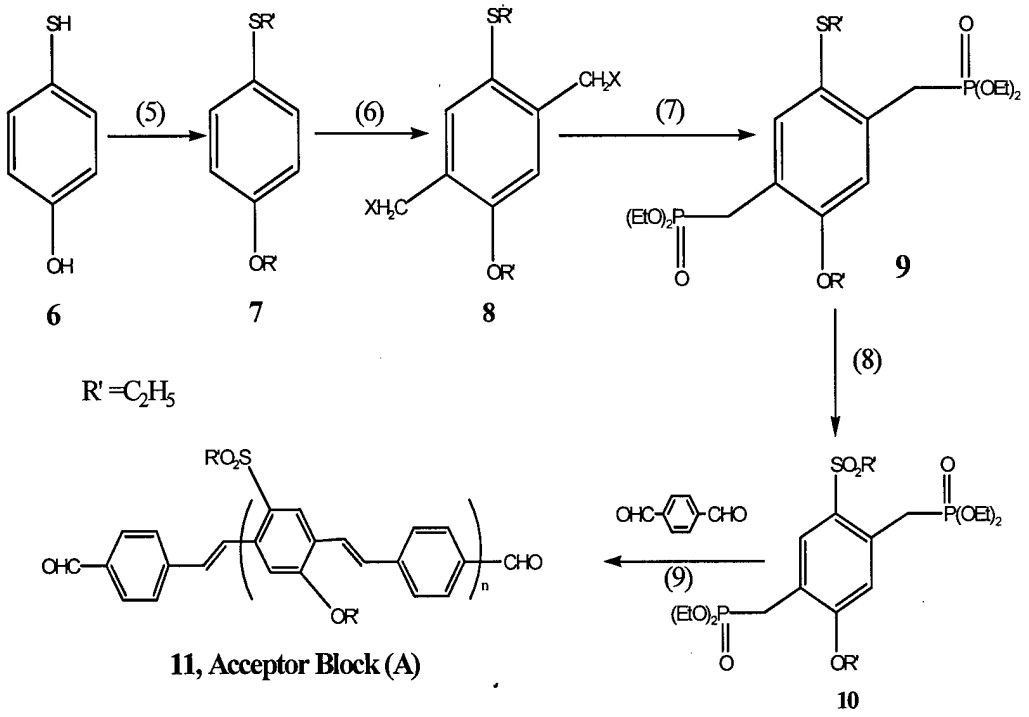

Figure A-7. Synthetic Scheme of an Acceptor Block (SF-PPV-I).

Step 1: 1-Ethoxy-4-ethylsulfanyl-benzene (Compound 7).

10 g (0.08 mol) of 4-Mercaptophenol **6** was mixed with 30 g KOH (excess) in 240 ml acetonitrile (CH_3CN) and 100 ml distilled water in a 500 ml 3-neck round flask. After 10 minutes of stirring, an ice bath was used to cool the reaction solution to 4 °C, then 30 ml bromoethane (excess) was added slowly. The reaction was kept in the original ice bath without adding new ice, and temperature slowly went up until it reached to room temperature. Reaction proceeded till TLC test (Hexane: Ethyl Acetate = 1:1) showed only one spot left (about 24 hours). After the reaction was stopped and cooled, the water layer and organic layer were separated. The organic layer was collected and directly put onto a rotary evaporator. After filtering of residue solid (KOH), 11.7g light yellow liquid 7 was obtained (yield: 95%). ^{1}H NMR ($CDCL_3$, ppm): 7.30 (d, 2H, phenyl), 6.85 (d, 2H, phenyl), 3.90 (m, 2H, -OCH_2), 2.95 (m, 2H, -SCH_2), 1.40 (m, 3H, -CH_3), and 1.20 (m, 2H, -CH_3).

$C_{10}H_{14}OS$ FW=182.28. Anal. Calcd for $C_{10}H_{14}OS$: C, 65.89; H, 7.74. Found: C, 65.91; H, 7.74.

Step 2: 1,4-Bis-bromomethyl-2-ethoxy-5-ethylsulfanyl-benzene (Compound 8).

5.0 g (0.027 mol) of **7**, 5.0 g para-formaldehyde $(CH_2O)_n$, 20 ml HBr (33 wt% in acetic acid), and 60 ml formic acid were mixed in a 250 ml 3-neck round flask under nitrogen atmosphere. The mixture was stirred and heated up to 65 °C. A white solid precipitated out after reacting 12 hours. The reaction was kept total 24 hours to achieve white solid state. After the reaction was stopped and cooled, the product mixture poured into 300 ml water, and the white solid **8** was collected by filtration followed by re-crystallization in methanol twice. 7.11 g of 3 was obtained (yield: 71%). ^{1}H NMR ($CDCL_3$, ppm): 7.35 (s, 1H, phenyl), 6.95 (s, 1H, phenyl), 4.40 (s, 2H, $-CH_2Br$), 4.25 (s, 2H, $-CH_2Br$), 3.90 (m, 2H, $-OCH_2$), 2.95 (m, 2H, $-SCH_2$), 1.40 (m, 3H, $-CH_3$), and 1.20 (m, 2H, $-CH_3$). $C_{12}H_{16}Br_2OS$ FW=368.13. Anal. Calcd for $C_{12}H_{16}Br_2OS$: C, 39.15; H, 4.38. Found: C, 39.29; H, 4.42.

Step 3: [4-(Diethoxy-phosphorylmethyl)-5-ethoxy-2-ethylsulfanyl-benzyl]-phosphoric acid diethyl ester (Compound 9).

7.11 g of **8** (0.00194 mol) and 6.46 g three ethyl phosphite $P(OEt)_3$ (0.0388 mol) were mixed together directly without any solvent and the temperature raised to 120 °C. When the temperature reached 80 °C, 3 started to melt. A short air-cooled condenser was used to allow the by-product, bromoethane, to escape from the system, so the reaction could be completed faster. After 24 hours, a liquid product **9** was further purified by high vacuum to remove remaining by-products. 9.35 g of **9** was obtained (yield: 100%). ^{1}H NMR ($CDCL_3$, ppm): 7.35 (s, 2H, phenyl), 6.95 (s, 1H, phenyl), 4.10-3.90 (m, 10H, $-OCH_2$, $-P(O)OCH_2-$), 3.45 (d, 2H, $-CH_2P-$), 3.25 (d, 2H, $-CH_2P-$), 2.95 (m, 2H, $-SCH_2-$), 1.40 – 0.95 (m, 18H, $-CH_3$). $C_{20}H_{36}O_7P_2S$ FW=482.51. Anal. Calcd for $C_{20}H_{36}O_7P_2S$: C, 49.78; H, 7.52. Found: C, 48.78; H, 7.54.

Step 4: [4-(Diethoxy-phosphorylmethyl)-2-ethanesulfonyl-5-ethoxy-benzyl]-phosponic acid diethyl ester (Compound 10).

9.35 g (0.0194 mol) of 9 and 100 ml glacial acetic acid was heated to 120 °C, then 3 g H_2O_2 (50 % in water) was added in 3 aliquots (10 mins each time). The temperature was

maintained and the mixture stirred for 12 hours. After the reaction was stopped, acetic acid and excess hydrogen peroxide were removed by the rotary evaporation. The remaining liquid was further purified by washing with aqueous NaOH solution and then by a short column (about 3 cm, chloroform was used as solvent) twice to remove small amount of residue acetic acid. ^{1}H NMR ($CDCL_3$, ppm): 7.98 (s, 1H, phenyl), 6.95 (s, 1H, phenyl), 4.10-3.90 (m, 10H, -OCH_2, -P(O)OCH_2-), 4.0-3.85 (m, 2H, -CH_2P-), 3.50-3.25 (m, 4H, -CH_2P-, -SO_2CH_2-), 1.40-0.95 (m, 18H, -CH_3). $C_{20}H_{36}O_9P_2S$ FW=514.51. Anal. Calcd for $C_{20}H_{36}O_9P_2S$: C, 46.69; H, 7.05. Found: C, 46.84; H, 7.04.

Step 5: SF-PPC-C_2H_5 having C_2H_5 side chain (Acceptor block 11).

0.274 g (2.02 mmol) of 1,4-benzene dicarboxaldehyde and 1.00 g [4-(Diethoxy-phosphorylmethyl)-2-ethanesulfonyl-5-ethoxy-benzyl]-phosponic acid diethyl ester **10** (1.99 mmol) were dissolved in 50 ml dry THF, and 0.44 g (0.018 mol) NaH in 20 ml anhydrous THF was added drop wise. The resulting reaction mixture was stirred for 24 hours at room temperature. After reaction was stopped, 30 ml methanol was added to quench the excess amount of NaH, and subsequently poured the mixture into 400 ml water. A bright orange colored and strongly luminescent solid was obtained by filtration. After dried in vacuum oven at 60 °C overnight, 0.52 g of **11** was obtained. ^{1}H NMR ($CDCL_3$, ppm): 8.20-7.90 (m, phenyl-H), 7.70-7.50 (m, phenyl-H), 7.40 (m, vinyl-H), 7.20-7.00 (m, phenyl-H), 7.00-6.80 (m, vinyl-H), 3.90 (m, -OCH_2-), 3.30 (m, -SO_2CH_2), 1.20-0.95 (m, -CH_3).

A-4. The Bridge Block

The purpose of using a non-conjugated bridge block is to separate conjugated donor block from the acceptor block. This will make the electrons and holes that are separated at the donor-acceptor interface more difficult to recombine. Also, different bridge block will affect the self-assemble ability as long as the solubility of the final block copolymers.

Figure A-8 shows two bridge blocks we have used in our donor-bridge-acceptor block copolymer system. The dialdehyde bridges were also synthesized. The diamine bridges were purchased from commercial sources.

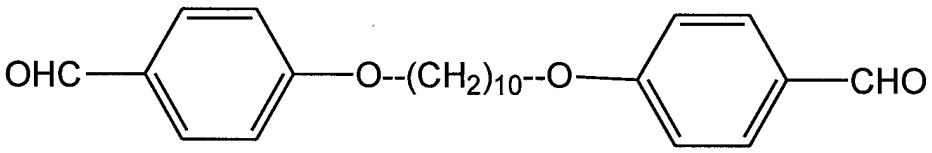

(a)

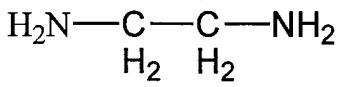

(b)

Figure A-8. Structures of Bridge Blocks.

NOTE:

We have tried to couple one bridge block with two aldehyde groups (B1) and one bridge block with two amine groups (B2). From table 2.2 shown below, one can see that the solubility and optical properties of the final –DBAB- block copolymers with two different bridge unit is almost the same. This is mainly because compared to the donor block and acceptor block, the bridge block is relatively small to affect those properties.

	H_2N-CH_2-CH_2-NH_2 (B2)	OHC-R_1-CHO (B1)
λex (nm)	480	490
λem (nm)	525	528
Solubility	Good	OK

Table A-2. -DBAB- Blokc Copolymer Properties versus Bridges.

A-5. Block Copolymer Synthesis.

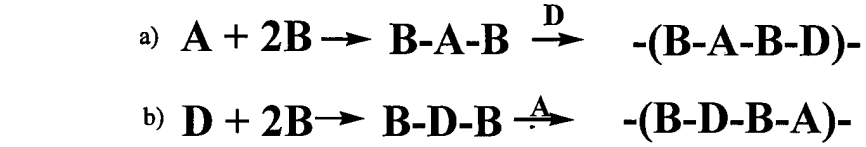

Figure A-9. General Synthetic Scheme of Block Copolymers.

The synthetic strategy of the final donor-bridge-acceptor block copolymer involves either use donor block or acceptor block to react with excess amount of bridge block to form the intermediates B-D-B or B-A-B, then acceptor block or donor block was added to form the final block copolymer.

For example, 0.5 g of **5** along with excess amount of diamine Bridge Block were dissolved in dry Toluene (50 ml). The mixture solution was allowed to stir for 48 h more under reflux. This solution was then poured into 500 ml methanol; the precipitates were collected and washed with water, and dried under vacuum. The B-D-B and the acceptor block **11** (calculated mole ratio is between 1:1 and 1:2) were then dissolved in 50 ml dry THF. The mixture was stirred under room temperature for 48 h before poured into 500 ml methanol. The precipitates were collected and dried under vacuum to get a red fluorescent solid, the final donor-bridge-acceptor block copolymer.

Notes:

In the synthesis of the donor-bridge-acceptor block copolymers, very dry solvent, THF or DMF, are required. If the solvent was not dried enough, the tiny water in the solvents may kill the base, which acts as a catalyst in the reaction. Therefore, the reaction may go very slow or not at all.

Even though the diamine bridge is a liquid, we still can not do a neat reaction without solvent. That is because the boiling point of the diamine bridge is well below the reaction temperature. And the solubility of the donor block and acceptor block in diamine bridge is not good.

Figure A-10 is the ^{1}H NMR spectra of the final block copolymer with diamine bridge. Compared with the ^{1}H NMR of donor block and acceptor block, the aldehyde peak, which originally appears at around 10 ppm in donor block and acceptor block's ^{1}H NMR spectra, became too weak to see. Also, other peaks that shown in donor block and acceptor block's ^{1}H NMR spectra can be found in that of the final tri-block copolymer and the ^{1}H peak of the bridge was overlapped by those alkene's peaks of donor block and acceptor block. ^{1}H NMR spectra δ (ppm): 0.89 (s, 30H, -CH3), 1.25 (m, 190H, -CH2-), 3.82 (m, 19H, -OCH2-, N-CH2-), 6.68 (s, 8H, aromatic), 7.15(m, 20H, -CH=CH-), 7.46 (t, 15H, aromatic). The ratio of the protons on the benzene ring and the aliphatic protons is somewhat deviate from calculation. Also, the aromatic peaks are weak. This may be caused by big volume of the final block copolymer molecules and the bulky size of the side chain that may shield the protons on the benzene ring.

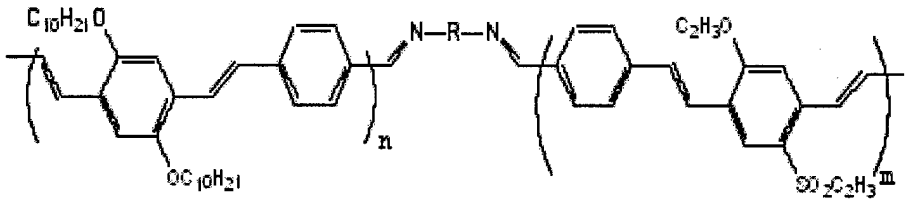

Structure of Donor-Bridge-Acceptor Block Copolymer

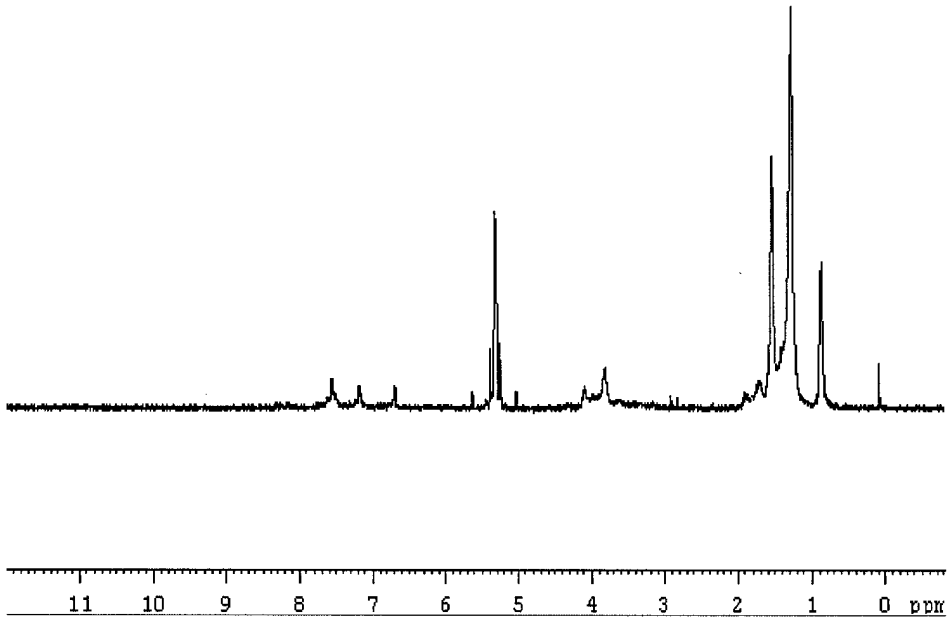

Figure A-10. ^{1}H NMR Spectra of a Final –DBAB- Block Copolymer.

The donor block and acceptor block, as well as the BDB and BAB block, were soluble in THF, while the synthesized BDBA block copolymers is only partially soluble in THF. Most notably, while the donor block or acceptor block were light yellow-reddish color in solid state with very strong luminescence, the synthesized final donor-bridge-acceptor block copolymers were brownish dark color in solid state, and was very weakly luminescence as will be discussed in later section. These also proved the successful coupling of donor block, bridge block and acceptor block.

The final block copolymers were characterized via ^{1}H NMR as well as GPC and MALDI, the MALDI results shows that the molecular weight of the donor-bridge-acceptor block copolymer is almost the sum of the donor block and acceptor block (the MW of bridge unit can be neglected). For example, from GPC analysis, the RO-PPV-C10 sample has an average molecular weight (Mw) of 3300 (13 phenylenevinylene monomer units, or 6 repeat units), after coupling with bridge $(CH_2NH_2)_2$ unit and SF-PPV-C2 of molecular

weight of 3000 (17 phenylenevinylene monomer units, 8 repeat units), the measured molecular weight of the final –DBAB- block copolymer is about 6500, slightly higher then the sum of the donor block and acceptor block. Both GPC and MALDI analysis shows a polymer molecular weight corresponding to one structure unit of D-B-A-B. Since the final block copolymer was only partially soluble in THF, and that filtering (0.2 μm) was applied before the polymer solution was analyzed with GPC, therefore, the GPC results only reflected the soluble part of polymer sample. There might be higher molecular weight block copolymers that are not soluble well in THF and was filtered out. MALDI analysis also confirmed the existence of at least a –D-B-A-B- unit. Though species with higher molecular weight than –D-B-A-B- were not obvious in MALDI data, however, it is also possible that higher molecular weight species may be broke down during laser ablation. There might be higher molecular weight block copolymers that were not soluble in THF and were filtered out. This is one of the reason we prefer to use –DBAB- which also include more repeat units instead of DBAB that indicates only one such unit.